SPACE RESEARCH INSTITUTE

IWF
Space Research Institute

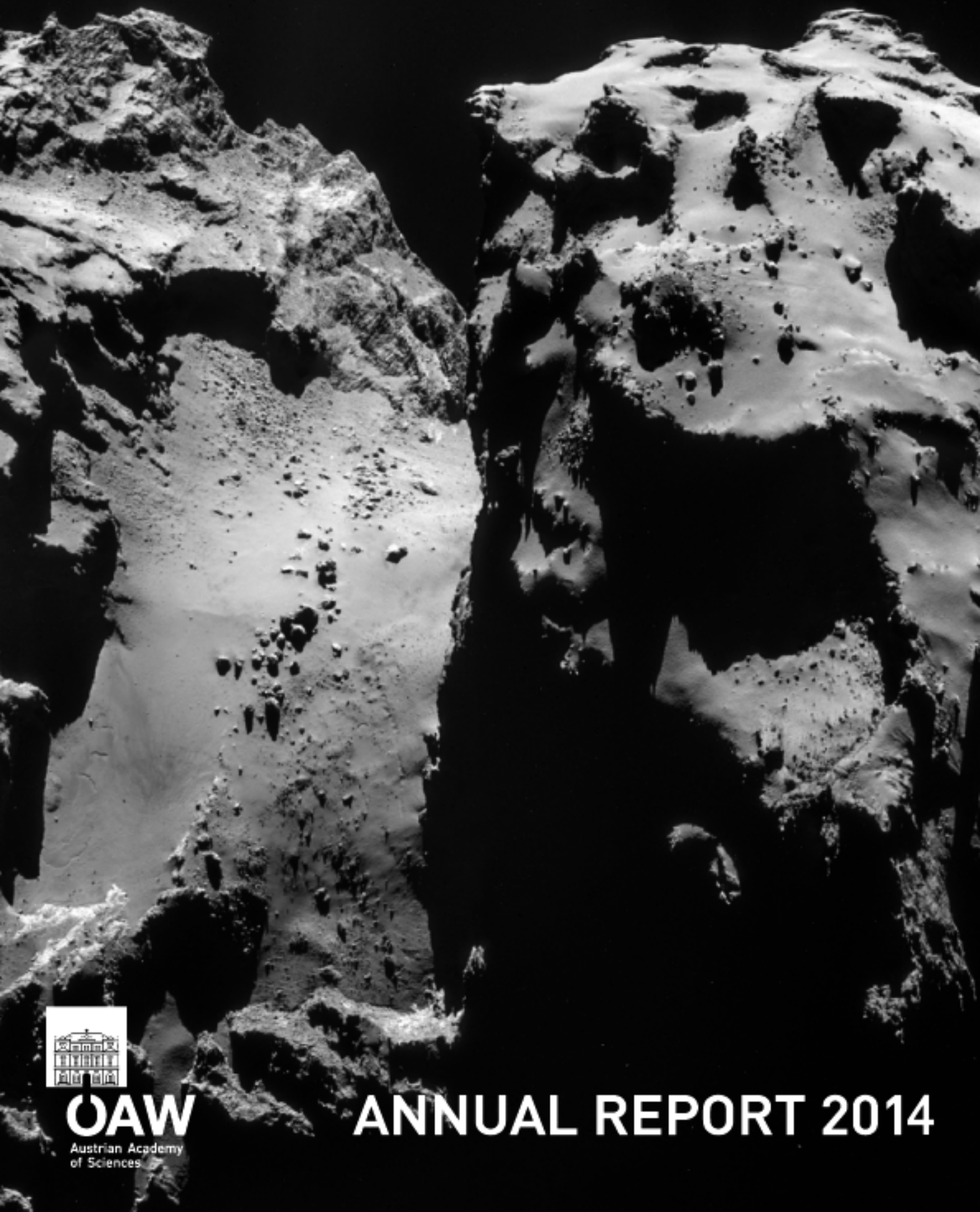

ÖAW
Austrian Academy of Sciences

ANNUAL REPORT 2014

IWF
Space Research
Institute

ANNUAL REPORT 2014

SPACE RESEARCH INSTITUTE GRAZ
AUSTRIAN ACADEMY OF SCIENCES

ÖAW
Austrian Academy
of Sciences

Cover Image

Comet 67P/Churyumov-Gerasimenko taken by Rosetta/NavCam on 9 December 2014 (Copyright: ESA/Rosetta/NAVCAM – CC BY-SA IGO 3.0).

Table of Contents

Introduction

The Space Research Institute (Institut für Weltraumforschung, IWF) of the Austrian Academy of Sciences (Österreichische Akademie der Wissenschaften, ÖAW) in Graz focuses on physics and exploration of the solar system, covering the whole chain of research needed in its fields: from developing and building space-qualified instruments to analyzing and interpreting the data returned by these instruments. With over 80 staff members of more than a dozen different nationalities it is the Austrian space research institute par excellence. It cooperates closely with space agencies all over the world and with numerous other national and international research institutions. A particularly intense cooperation exists with the European Space Agency (ESA).

In terms of science, IWF concentrates on space plasma physics, on the upper atmospheres of planets and exoplanets, and on the Earth's and the Moon's gravity field. In the area of instrument development the focus lies on building magnetometers and on-board computers, on antenna calibration, and on satellite laser ranging.

Presently, the institute is involved in sixteen international space missions:

- *BepiColombo* will be launched in 2017 to investigate planet Mercury, using two orbiters, one specialized in magnetospheric studies and one in remote sensing.
- *Cassini* will continue to explore Saturn's magnetosphere and its moons until 2017.
- ESA's first S-class mission *CHEOPS (CHaracterizing ExOPlanets Satellite)* will characterize exoplanets in detail. Its launch is expected in 2017.
- The *China Seismo-Electromagnetic Satellite (CSES)* will be launched in 2016 to study the Earth's ionosphere.
- *Cluster*, ESA's four-spacecraft mission, is still providing unique data leading to a new understanding of space plasmas.
- *InSight (INterior exploration using Seismic Investigations, Geodesy and Heat Transport)* is a NASA Discovery Program mission that will place a single geophysical lander on Mars to study its deep interior. It is expected for launch in 2016.
- ESA's *JUpiter ICy moons Explorer (JUICE)* will observe the giant gaseous planet Jupiter and three of its largest moons, Ganymede, Callisto, and Europa. It is planned for launch in 2022.
- *Juno* is a NASA mission dedicated to understand Jupiter's origin and evolution.
- *MMS* will use four identically equipped spacecraft to explore the acceleration processes that govern the dynamics of the Earth's magnetosphere (launch in March 2015).
- *Resonance* is a Russian space mission of four identical spacecraft, orbiting partially within the same magnetic flux tube, scheduled for launch in 2015.
- *Rosetta* arrived at comet 67P/Churyumov-Gerasimenko in August and deposited its lander *Philae* in November 2014.
- *Solar Orbiter* is to study along an innovative trajectory solar and heliospheric phenomena, planned for launch in 2018.
- *STEREO* studies solar (wind) structures with two spacecraft orbiting the Sun approximately at Earth's distance.

- *THEMIS* has been reduced to a near-Earth three-spacecraft mission. The two other spacecraft are now orbiting the Moon in the *ARTEMIS* mission.
- The *Van Allen Probes* are two NASA spacecraft, which will quantify processes in the Earth's radiation belts.
- *Venus Express* explored the space plasma environment around Venus and ended its mission in December 2014.

IWF is naturally engaged in analyzing data from these and other space missions. This analysis is supported by theory, simulation, and laboratory experiments. Furthermore, at Lustbühel Observatory, one of the world's most accurate laser ranging stations is operated.

Highlights in 2014

- Using Lyman-α observations of HD209458b and modeling the absorption features it was found that this exoplanet has a magnetic moment a thousand times stronger than the Earth.
- The validity of using solar pseudo indices for reproducing the influence of extreme solar flares on the Earth's thermosphere has been shown.
- The core field direction for magnetic flux ropes created in the Earth's magnetotail was shown to correlate only with the solar wind magnetic field for strong reconnection guide fields.

The year 2014 in numbers

Members of the institute published 113 papers in refereed international journals, of which 38 were first author publications. During the same period, articles with authors from the institute were cited more than 3100 times in the international literature. In addition, 129 talks and 50 posters have been presented at international conferences by members of the IWF, including 22 by special invitation from the conveners. Last but not least, institute members organized and chaired 21 sessions at 10 international meetings.

IWF structure and funding

IWF is, as a heritage since foundation, structured into three departments:

- Experimental Space Research
- Extraterrestrial Physics
- Satellite Geodesy

Wolfgang Baumjohann serves as Director. Scientifically, there are no walls between the three departments. Staff members from different departments work successfully together in five research fields (Fig. 1).

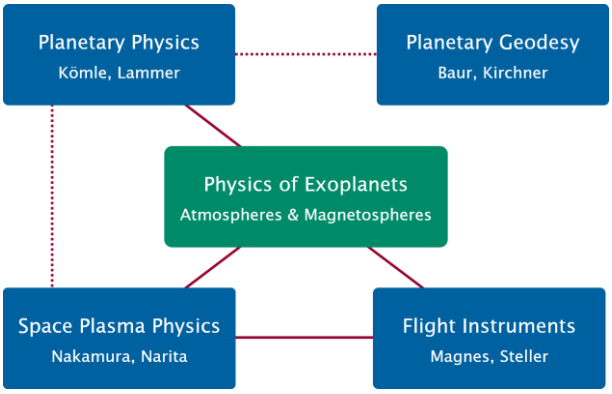

Fig. 1: IWF research fields and group leaders.

The bulk of financial support for the research is provided by the ÖAW. Substantial support is also provided by other national institutions, in particular the Austrian Research Promotion Agency (Österreichische Forschungsförderungsgesellschaft, FFG) and the Austrian Science Fund (Fonds zur Förderung der wissenschaftlichen Forschung, FWF). Furthermore, European institutions like ESA and the European Union contribute substantially.

Earth & Moon

Gravimetric and geometric space geodesy techniques constitute an integral part in Earth and planetary sciences. In order to improve our knowledge about the environment, state and evolution of the Earth and the Earth's only natural satellite, the Moon, IWF is engaged in terrestrial and lunar gravity field research, selected studies of the Earth's atmosphere and crustal dynamics, and Satellite Laser Ranging (SLR) to Earth-orbiting spacecraft and debris objects.

Gravity Field

Gravity field research includes the analysis of data collected by Earth- and Moon-orbiting spacecraft and SLR to passive satellites.

GOCE

IWF together with the Institute of Theoretical Geodesy and Satellite Geodesy of the Graz University of Technology form the *Gravity field and steady-state Ocean Circulation Explorer (GOCE)* team Graz, which processes the official *GOCE* time-wise (*GOCE*-TIM) gravity field solutions. This unit is part of the European *GOCE* Gravity Consortium, which consists of ten European institutions working under ESA contract. In 2014, the fifth generation *GOCE*-TIM gravity field solution has been released to the public by ESA. This model contains data from Nov 2009 to Oct 2013 (and hence covers almost the entire *GOCE* operational lifetime). At 100 km spatial resolution (spherical harmonic degree and order 200), the accuracy is 2.3 cm and 0.7 mGal in terms of geoid height and gravity anomaly, respectively. This is an improvement of about 30% compared to the predecessor model.

GRACE

In the last decade, global time-variable gravity field observations collected by the *Gravity Recovery And Climate Experiment (GRACE)* mission have become an indispensable source of information for understanding the global redistribution of ice, ocean, and continental water mass (cf. latest Assessment Report of the Intergovernmental Panel on Climate Change, IPCC-AR5). However, the *GRACE* satellites have already outlived their predicted lifetime and may fail at any time (successor is supposed to be launched in 2017).

Hence, time-variable gravity field information derived solely from the GPS-based kinematic orbits of low Earth-orbiting satellites, known as high-low Satellite-to-Satellite Tracking (hlSST), has recently received renewed attention. Owing to striking developments to improve the underlying processing chain, it is now possible to detect and quantify large-scale changes in surface mass from hlSST (Fig. 2).

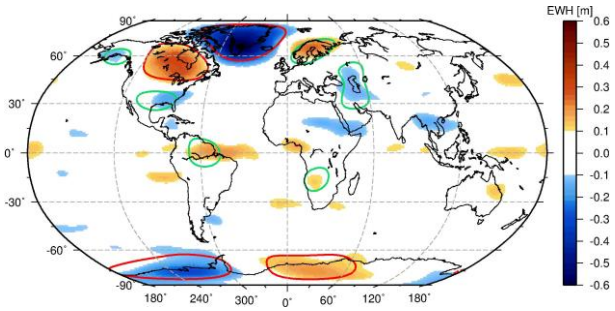

Fig. 2: Secular mass change in terms of equivalent water height over the period 2003-2013, derived from hlSST. Red delineations highlight areas with dominating signals.

The results shown in Fig. 2 are in very good agreement with the findings from the *GRACE* project. In terms of numbers, trends agree with 85-100% (red-delineated areas).For the annual amplitudes, the level of agreement is 85-95%.

GOCO

The main objective of the *Gravity Observations COmbination (GOCO)* initiative is to compute high-accuracy and high-resolution global gravity field models from complementary gravity data sources. Within this initiative, IWF is responsible for the Satellite Laser Ranging (SLR) component. SLR is a powerful technique for the estimation of the very long wavelengths of the Earth's gravity field. The most important parameter in this context is C_{20}. It represents the Earth's dynamic flattening, which is responsible for the largest deviation of the real figure of the Earth from its spherical approximation. Despite of having available data from a number of dedicated gravity field missions, SLR is still superior for the determination of C_{20} (Fig. 3). However, the technique also significantly contributes to the recovery of further low-degree gravity field parameters. At IWF, ranging measurements to six geodetic satellites *(LAGEOS-1/2, Stella, Starlette, Ajisai, Larets)* over a period of nearly 15 years were analyzed.

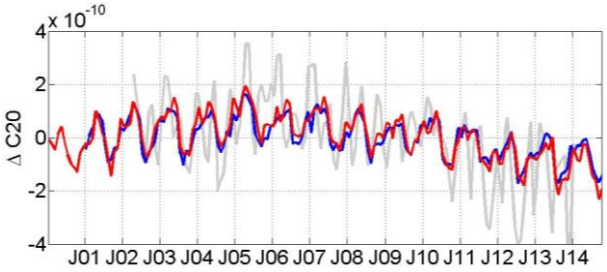

Fig. 3: Monthly C_{20} gravity field coefficients (reduced by mean values) derived from SLR (red: IWF; blue: Center for Space Research, CSR) and the GRACE mission (gray).

According to Fig. 3, the SLR-based solutions show very good agreement, whereas the *GRACE* C_{20} time series reveals unrealistically large amplitudes. This result demonstrates the superiority of SLR when it comes to the determination of the Earth's dynamical flattening. The next combined gravity field model within the *GOCO* series *(GOCO05s)* will contain SLR information up to spherical harmonic degree and order 10. The model is expected to get published in early 2015.

LRO

Tracking data to NASA's *Lunar Reconnaissance Orbiter (LRO)* spacecraft – launched in 2009 – is well suited to determine the long-wavelength part of the lunar gravity field. This holds especially true for a time span of two years, when the orbit of *LRO* was polar (global coverage) with an altitude of about 50 km above the lunar surface. Gravity field recovery from orbit perturbations is intrinsically related to precise orbit determination. In case of *LRO*, two types of tracking data are available: radiometric observations (mainly two-way Doppler range-rates and radiometric ranges) and one-way optical laser ranges. The optimum set of orbit modeling parameters was found by a series of orbit overlapping tests based on 100 days of Doppler data. The most precise orbits were achieved using an arc length of 2.5 days and estimating a constant empirical acceleration in along-track direction. Altogether, 13 months of Doppler data to *LRO* were analyzed. Orbit overlap differences over this time span indicate an orbital precision of about 20 m in total position. Orbit determination from laser ranges yielded considerably less precise results, which can be attributed to the involvement of two non-synchronous clocks (one at the station and one aboard the satellite). Hence, the *LRO* gravity field solution (up to spherical harmonic degree and order 60) computed at the IWF is based solely on Doppler range-rates. Starting at degree six, regularization was applied due to the lunar farside data gap (see Fig. 4).

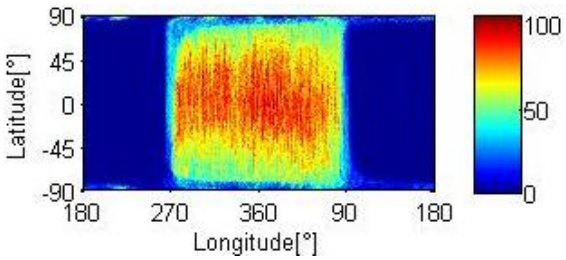

Fig. 4: Total number of Doppler range-rates to LRO within one year, averaged over a 1°x1° grid. The western limb of the Moon as seen from the Earth is located at 270°. The asymmetric data availability is due to Moon's tidal lock.

GRAIL

The NASA lunar science mission *Gravity Recovery And Interior Laboratory (GRAIL)* uses Ka-Band Range-Rate measurements (KBRR) between two satellites in order to resolve the lunar gravity field with unprecedented resolution and accuracy. This satellite-to-satellite tracking technique is independent of the tracking capability from Earth, thus allowing data acquisition on the nearside and the farside of the Moon.

To determine the lunar gravity field, KBRR observations (together with orbit information) were analyzed within an integral equation approach using short orbital arcs. For the latest release (denoted as Graz Lunar Gravity Model 300a, or GrazLGM300a) particular attention was paid to processing details associated with time bias estimation, the modelling of non-gravitational forces, and the co-estimation of empirical accelerations (aka nuisance parameters). GrazLGM300a considers non-gravitational accelerations due to solar radiation pressure and general relativity (Schwarzschild); a comparison between this latest release with some other lunar gravity field models is shown in Fig. 5.

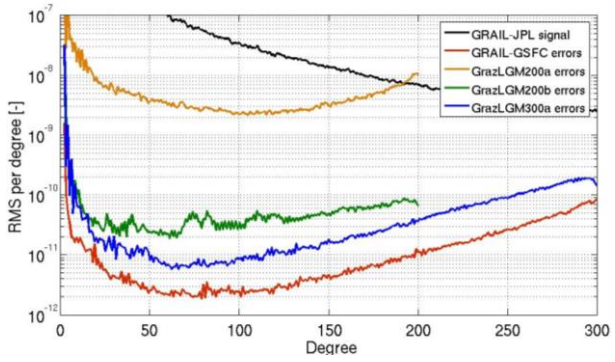

Fig. 5: Root mean square (RMS) values per spherical harmonic degree. Black graph: GL0660 signal; color graphs: differences to GL0660.

The black graph indicates the signal of the GL0660 model computed at NASA-JPL; the red graph represents deviations from the GRGM660 model computed at NASA-GSFC. The latter graph can be considered as the "baseline errors". The GrazLGM300a model shows clearly a significant improvement compared to the previous releases (GrazLGM 200a,b).

Geodynamics

At the Earth's surface minor and major plates are moving against each other. At their boundaries stress is frequently released into earthquakes. The energy potential to be released can be estimated by the stress accumulated and the mass of the part of the Earth's crust under stress. Therefore a velocity field is necessary for a permanent control of the potential stress accumulations. An example of the zone with the strongest earthquakes in Europe is shown in Fig. 6. The earthquake with its epicenter in the Aegean Sea between Samothraki and Lemnos (magnitude: 6.9, depth: 6.5 km), recorded on 24 May 2014, caused damages and injuries at distances of more than 100 km.

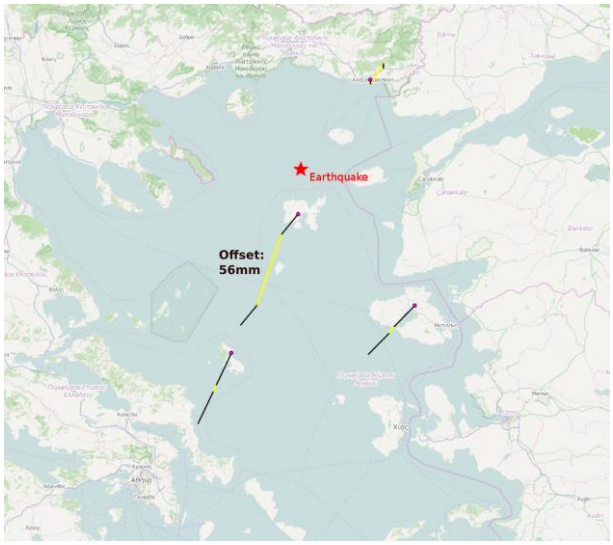

Fig. 6: Implications of the earthquake from 24 May 2014, with epicenter in the Northern Aegean Sea. Yellow: remanent offsets, black: station velocities.

As illustrated in Fig. 6, the earthquake implicated a permanent jump of 56 mm near the epicenter, decreasing to a few mm at distances of 100 km. This means that the stress release was only a local one, but the underlying plate (probably the compact Anatolian one) accumulates the stress in the neighborhood. Especially in the area of Greece the fragmentation of the diverse plates and microplates requires a

dense GNSS-derived velocity field in order to improve local and regional tectonic models. This will help to learn more about the nature and occurrence of earthquakes.

Atmosphere

Part of the solar wind energy supplied to the Earth's magnetosphere is deposited into the thermosphere via particle precipitation and Joule heating. During periods of high Coronal Mass Ejection (CME) activity, short-timescale variations (1-2 days) in the thermosphere are driven by magnetospheric energy input rather than by variations in the solar EUV flux. To quantify the large-scale response of the thermospheric neutral density to the energy input by interplanetary CMEs (ICMEs), a statistical study based on accelerometer measurements from the low-Earth orbiting *GRACE* satellites during 2003-2010 was performed. In addition, correlations with data from the *ACE* satellite located at L1 upstream of the Earth and various geomagnetic activity indices were calculated. By analyzing the data, high correlations between the neutral density and various combinations of ICME parameters could be found. The highest correlation coefficient (cc) is between density and Disturbance storm time (Dst) index (cc=-0.91), Fig. 7. Similarly, the product Bz*vmax reveals a high correlation with density (cc=-0.84).

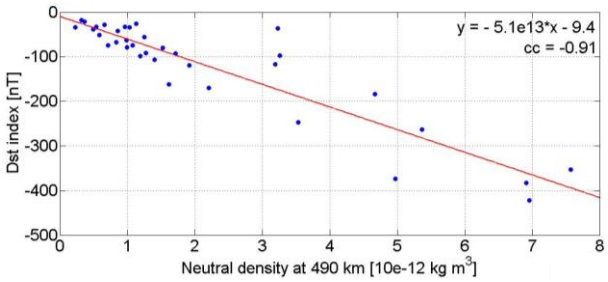

Fig. 7: Scatter plot of the peak thermospheric density against the Dst index. Red: regression line.

A substantial part of ICMEs arriving at the *ACE* satellite cause an increase of the neutral density in the Earth thermosphere. Furthermore, 31 out of the 35 analyzed ICME events show typical characteristics of magnetic clouds, including a smooth rotation of the magnetic field vector. Nearly all ICMEs causing a thermospheric density enhancement have a strong negative Bz component.

Satellite Laser Ranging

The continuing routine tracking of satellites equipped with retro-reflectors (in coordination with the International Laser Ranging Service, ILRS) again has proven to be the basis for several research activities. Most of the scientific achievements and results take advantage of the Graz kHz ranging system. Furthermore, tracking of space debris objects was continued, as well as further steps were undertaken to realize multi-static SLR making use of receive-only units.

Satellite spin detection: The 2 kHz SLR system in Graz is an excellent tool to determine spin parameters of retro-reflector equipped satellites. In 2014 all available tracking data to the satellites *Larets* and *Stella* were used to determine their spin parameters (Fig. 8). In addition, the evolution of the spin axis orientation for *Larets* and *Stella* could be successfully recovered (Fig. 9).

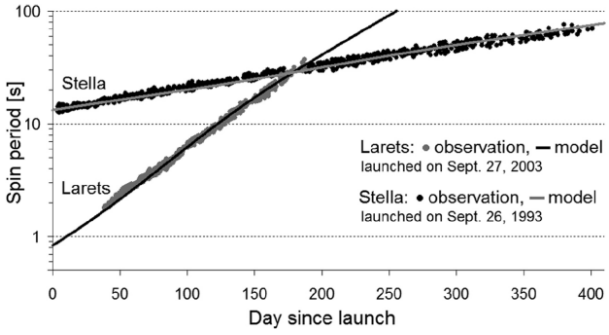

Fig. 8: Spin period evolution of the geodetic satellites Larets and Stella.

Single-photon DART for multi-static space debris tracking: More participating passive (receive-only) units are needed for efficient multi-static SLR. This can be achieved by using available standard astronomy telescopes and equipping them with proper single-photon de-

tection packages, electronics, additional hardware, and remote control. To check proper alignment of the detector and to verify single-photon sensitivity, the development of a Single-Photon Detection, Alignment and Reference Tool (SP-DART) was initiated. Effectively, this is a miniature SLR-station, which consists of a transmitter unit (few µJ laser, few ns pulse duration, 1 kHz pulses), a detection unit, a range gate generator (FPGA card), a set of meteorological instruments, a GPS clock and reference frequency receiver, software, and remote control via Internet. Once the currently ongoing developing phase is finished, the unit is expected to be mounted on external astronomy telescopes and used to verify their single-photon sensitivity. The SP-DART system will be designed and built for two wavelengths – 532 nm and 1064 nm – in order to allow for tests at both fundamental and second harmonic wavelengths.

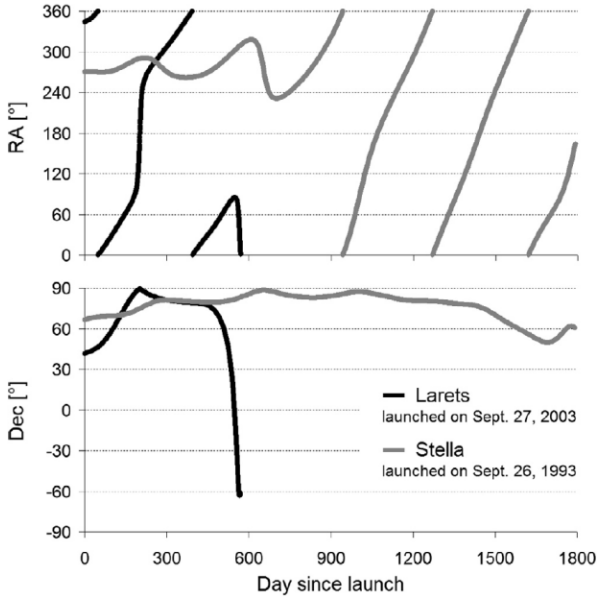

Fig. 9: Larets (black) and Stella (gray) spin axis orientation: evolution from launch until resonance condition (J2000.0 celestial reference frame). RA and Dec indicate the astronomical coordinates right ascension and declination, respectively.

Space debris attitude and spin determination:

IWF started to measure attitude and spin parameters of a large number of defunct satellites and space debris objects (currently the number of objects is 55, but being updated continuously). This activity has increased the number of targets tracked by the Graz SLR-station to 116, which is almost three times the number of targets recommended by the ILRS to be tracked. In order to be able to handle the resulting large numbers of passes per day, appropriate pass switching capabilities were further improved (Fig. 10). As soon as at least 1000 echoes are detected (reaching our ultimate 0.2 mm resolution of the system), the next target is tracked; multiple entries into each pass ensure to cover an as large section of the pass as possible.

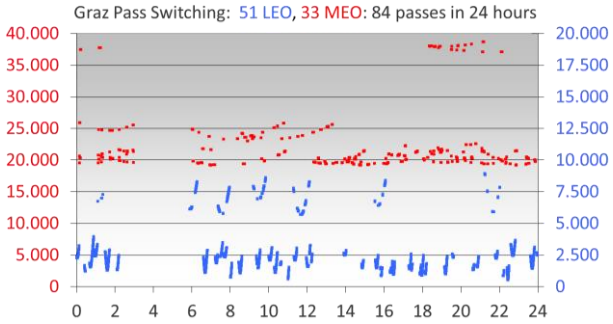

Fig. 10: Extensive pass switching in Graz (day 266 in 2014). Red: Medium-Earth Orbit, blue: Low-Earth Orbit; y-axis displays orbit satellite altitude above surface.

The major part of these debris targets are old, defunct *GLONASS* satellites. When uncontrolled, they usually start spinning. Because of their retro-reflectors, which are only visible during short intervals, SLR is the only practicable method to reliably allow for spin and attitude determination (Fig. 11).

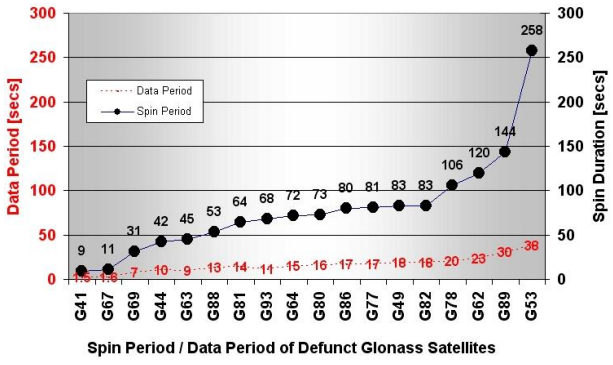

Fig. 11: Spin rates of defunct GLONASS satellites as observed by SLR Graz.

Another example of a relatively fast spinning defunct satellite is *Topex/Poseidon*. It is spinning with 11.81 s/rev (value from end of 2014),

with its spin axis orientation fixed with respect to Earth, showing its retro-reflectors throughout the pass. This allows tracking of *Topex/Poseidon* also during daylight, in spite of the rather inaccurate two-line element predictions.

New Detection Package: Experiments planned for the coming years require the addition of at least six more detectors, for different wavelengths and with different specifications. To accommodate the additional units – and their remote controlled activating, switching of filters and mirrors, etc. – a new detection box was designed and built, and finally mounted on the Graz receive telescope. This new detection package is successfully operational since autumn 2014.

Quantum cryptography: The Institute for Quantum Optics and Quantum Information (IQOQI) has designed and built a 4-channel package to detect entangled photons transmitted from a Chinese Quantum Cryptography satellite to be launched in 2016. During several visits of the IQOQI group in Graz this package has been installed and tested with the Graz SLR telescope. After several iterations and improvements to come, the package is expected to be ready for operation towards the end of 2015.

Orbit prediction of space debris objects: Large and massive space debris objects in the low-Earth orbit segment pose an increasing threat to all space faring nations. For collision avoidance measures or the removal of these objects, orbit predictions are of crucial relevance. It has recently been demonstrated that laser ranging has the potential to significantly contribute to the reliability and accuracy of orbit predictions. However, a severe limitation of the technique is the scant network of SLR stations that are able to track uncooperative targets, and hence the sparseness of tracking data. In order to mitigate this limitation, the concept of multi-static SLR has been established. Multi-static observations refer to the tracking of objects from one active SLR-station and the detection of diffusely reflected photons at several passive stations. If only one passive station is involved, the concept is referred to as bi-static.

In order to demonstrate the benefit of bi-static SLR for orbit determination and prediction of the defunct *ENVISAT* satellite, observations collected during a measurement campaign with involved stations Graz (active) and Wettzell (passive) were analyzed. It could be demonstrated that the incorporation of bi-static laser observations improves the prediction accuracy by more than one order of magnitude compared to the results based on "conventional" two-way laser ranges collected by only one station (Fig. 12).

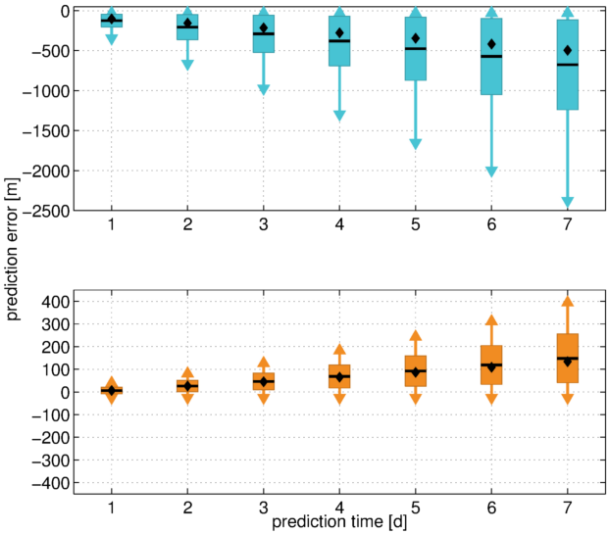

Fig. 12: Orbit prediction errors for the defunct ENVISAT satellite. Top: results based on Graz-only "conventional" two-way laser ranges; bottom: results after inclusion of bi-static laser observations between Graz and Wettzell.

Near-Earth Space

Near-Earth space is an ideal natural laboratory to study space plasmas physics with in-situ measurements of the charged particles together with electric and magnetic fields. IWF both builds instruments for satellite missions that make measurements in this natural laboratory and analyzes the data obtained by them, and participates in future planning.

Cluster

The four *Cluster* spacecraft have been providing data since 2001 for studying small-scale structures of the magnetosphere and its environment in three dimensions. The spacecraft separation distance has been varied between 200 km and 10 000 km according to the key scientific regions. The mission is planned to be extended to December 2018. IWF is PI/Co-I on five instruments.

THEMIS/ARTEMIS

NASA's *THEMIS* mission, launched in 2007, consisted of five identical satellites flying through different regions of the magnetosphere. In autumn 2010 the two outer spacecraft became *ARTEMIS*, while the other three *THEMIS* spacecraft remained in their orbit. As Co-I of the magnetometer, IWF is participating in processing and analyzing data.

Van Allen Probes

The *Van Allen Probes* launched in 2012, are studying the dynamics of the radiation belts. As one of the science Co-I institutes, IWF participates in data analysis combined with other magnetospheric missions.

MMS

NASA's *MMS* mission *(Magnetospheric Multi-scale)* will explore the dynamics of the Earth's magnetosphere and its underlying energy transfer processes. Four identically equipped spacecraft are to carry out three-dimensional measurements in the Earth's magnetosphere. *MMS* will determine the small-scale basic plasma processes, which transport, accelerate and energize plasmas in thin boundary and current layers. IWF is the biggest non-US participant and has the lead for the spacecraft potential control *(ASPOC)* and participates in the electron beam instrument *(EDI)* and the digital fluxgate magnetometer *(DFG)*. *MMS* is scheduled for launch in March 2015. In April 2014, all four of the *MMS* observatories were stacked for the first time for vibration testing. The test helped to ensure the spacecraft can withstand the extreme vibration and dynamic loads they will experience inside the fairing during launch (Fig. 13).

Active Spacecraft Potential Control (ASPOC) instrument: In January 2014, the FM1 unit faced a hardware failure in the hot cycle of the thermal vacuum test. The cause was a DPU board problem and it was decided to replace the instrument by the FM9 spare unit. After the refurbishment and partial re-qualification of FM9 in March, four additional thermal cycles have been performed in order to compensate for operating hours that were missed from the test. Before delivery of the FM9 unit to the US in June, the data package was compiled and reviewed. All models passed the complete sequence of comprehensive performance testing,

stack vibration, thermal vacuum, EMC, and magnetic tests on observatory level. The flight version of the on-board S/W was loaded into all units and the command and telemetry database was updated.

A further focal point in 2014 was the planning and implementation of the nine *ASPOC* commissioning activities, which include low/high voltage and cross-instrument checkouts. Each activity comprises several command sequences, which have been tested on instrument and observatory level. In order to support the commissioning phase, the ground system equipment has been installed in Boulder. Finally, the science data processing software, used for the automatic generation of the *ASPOC* level 1/2 science data products, has been implemented, tested and delivered to the Science Operations Center.

Electron Drift Instrument (EDI): IWF contributes to *EDI* with the *Gun Detector Electronics (GDE)* and the electron gun. The *GDE* is developed by Austrian industry in close cooperation with the institute, while the electron gun is entirely developed by IWF. MMS' *EDI* is based on the *Cluster* development with several improvements. In 2014 the last four flight models were delivered and one model has been refurbished with a new type of optocouplers. The generation and the control of the electron beam require twenty controllable high-voltage sources, which deliver relatively low power, but need high precision, controlled by in-house developed high-voltage optocouplers. A few couplers developed a negative drift in efficiency. US team-built replacements, based on the same principle, but slightly changed design, showed the same behaviour after intensive testing. Four gun models have been equipped with the new, less-efficient, type; the gradient of the drift seems to be smaller.Analysis showed both types will be able to cover the nominal operation time. Finally, all eight instruments have been tested successfully and integrated onto the four spacecraft.

Fig. 13: All four stacked Magnetospheric Multiscale spacecraft ready to move to the vibration chamber at NASA's Goddard Space Flight Center. (Credits: NASA/Chris Gunn).

Digital FluxGate magnetometer (DFG): *DFG* is based on a triaxial fluxgate magnetometer (FGM) developed by the University of California, Los Angeles, and a front-end Application Specific Integrated Circuit (ASIC) for magnetic field sensors. The ASIC has been developed by IWF in cooperation with the Fraunhofer Institute for Integrated Circuits in order to reduce size, mass and power consumption of the near sensor electronics. In 2014, the DFG spare model was delivered to University of New Hampshire. Parallel to the final hardware assembly activities, IWF supported the spacecraft integration of the flight models with all related functional tests.

Cross Calibration: Methods for determining spin axis offset of the *FGM* using absolute magnetic field values deduced from *EDI* are further improved by using both data of the time-of-flight (TOF) measurements and the

electron beam direction (BD) with a comprehensive error analysis. Both methods are successfully applied to *Cluster* data (Fig. 14), yielding similar, accurate results, comparable to, yet more stable than those from a commonly used solar wind (SW)-based method.

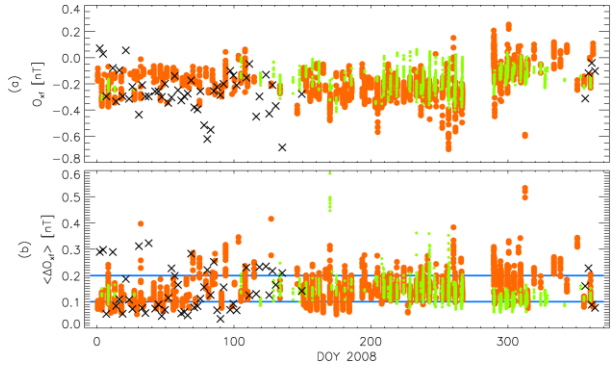

Fig. 14: (a): Spin axis offsets O_{xf} obtained by the TOF (red dots), the BD (green dots), and the SW method (black crosses). (b) Corresponding average errors, $<O_{xf}>$. The blue lines mark $<O_{xf}>$ = 0.1 nT and 0.2 nT levels.

CSES

The *China Seismo-Electromagnetic Satellite (CSES)* mission is scheduled for launch end of 2016 and will be the first Chinese platform for the investigation of natural electromagnetic phenomena with major emphasis on earthquake monitoring from a Sun synchronous, polar, Low Earth Orbit (LEO).

Fig. 15: Engineering Model of the Coupled Dark State Magnetometer.

The *CSES* magnetometer is developed in cooperation between the Center for Space Sciences and Applied Research (CSSAR) of the Chinese Academy of Sciences, IWF and the Institute of Experimental Physics of the Graz University of Technology (TUG). CSSAR is responsible for the dual sensor fluxgate magnetometer, the instrument processor and the power supply unit, while IWF and TUG participate with the newly developed absolute scalar magnetometer called *CDSM*. In 2014, the Engineering Model (Fig. 15) was delivered to China and the assembly of the Qualification Model was started.

Space Weather Magnetometer

A prototype of a *Service Oriented Spacecraft Magnetometer (SOSMAG)* is being developed for ESA's Space Situational Awareness program, which shall serve as a ready-to-use space weather monitoring system to be mounted on a variety of different spacecraft built without a magnetic cleanliness program (Fig. 16).

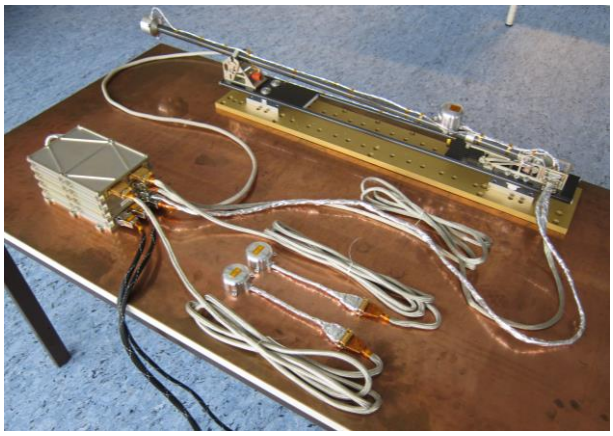

Fig. 16: Engineering and Qualification Model of SOSMAG.

Up to two high resolution boom-mounted FGMs, the central electronics and the boom are provided by Magson GmbH and the Technical University of Braunschweig. For detection and characterization of magnetic disturbers on the spacecraft, two magnetometers based on the anisotropic magnetoresistive (AMR) effect were developed in a joint effort by Imperial College London and IWF.

Physics

Various data from ongoing missions are analyzed and theoretical models are developed to describe the physical processes in near-Earth space. The studies deal with interactions between solar wind and magnetosphere, internal disturbances in the magnetosphere such as

plasma flows and waves, and plasma instabilities including magnetic reconnection.

Multi-spacecraft observations of magnetosheath high speed jets: The Earth's magnetic field acts as an obstacle to the solar wind. As a result, the solar wind is decelerated at the bow shock and flows in the magnetosheath around the magnetosphere. The dynamic pressure in the dayside magnetosheath is typically an order of magnitude lower than in the solar wind. Under radial interplanetary magnetic field conditions, however, this region of space is permeated by localized (high-speed) jets, within which the dynamic pressure is substantially higher. These jets are able to cause large indentations of the magnetopause – the outer boundary of the Earth's magnetic field – resulting in boundary surface waves and/or inner-magnetospheric compressional waves.

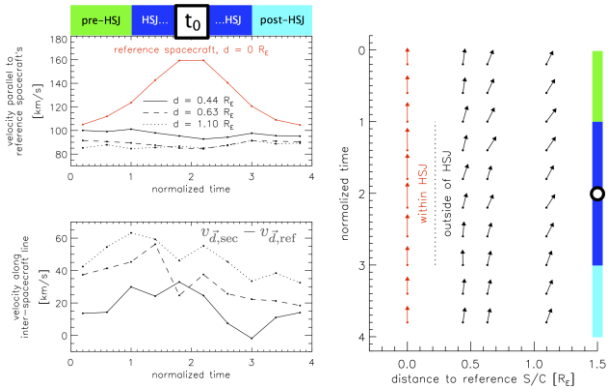

Fig. 17: Left: Top/bottom panels show jet-parallel/perpendicular plasma flows, observed by reference (inside) and second spacecraft (outside of jets). Right: illustration of the average flow pattern.

A key ingredient of the jet's geoeffectiveness is its size (relative to the magnetosphere). For the first time, multi-spacecraft observations by the *THEMIS* spacecraft allow for a determination of jet scale sizes and plasma flow patterns within and around jets. Scales are well-modeled by exponential probability distribution functions (Fig. 17). Characteristic flow-perpendicular scales are, interestingly, almost twice as large as the corresponding flow-parallel scales. Furthermore, the observed flow-parallel scale sizes become larger with distance from the bow shock, possibly due to early dissipation of small scale jets, closer to the bow shock. The plasma flow pattern (in- and outside of jets) exhibits additional/less divergence ahead of/after jet passage, corresponding to vortical plasma motion.

Core field polarity of flux ropes in magnetotail reconnection region: Magnetic flux ropes have a helical magnetic field structure, which typically has a significant core field (i.e., the component of the magnetic field along the axis of the flux rope). They are considered to be the by-products of reconnection.

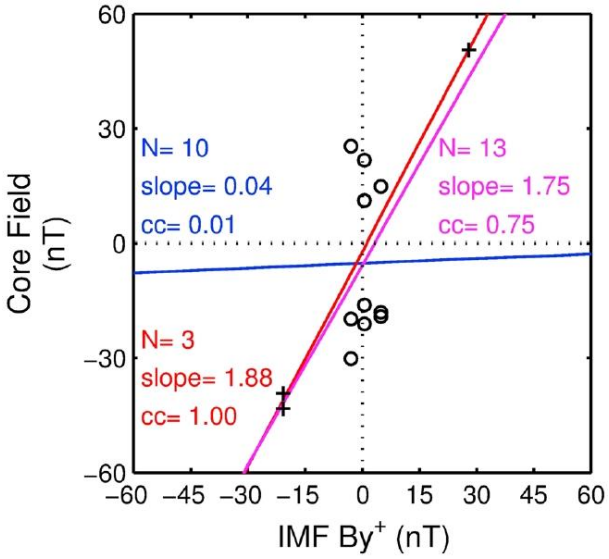

Fig. 18: Core field versus IMF By+ for the 13 flux ropes. The circles (pluses) denote the flux ropes with weak (large) guide fields. The core field of the 13 flux ropes showed dependence on IMF By+ (regression line shown in magenda). Yet, strong correlation is seen only for the flux ropes with large guide fields (regression line in red), while there is no correlation between the core field and IMFBy+ for flux ropes with weak guide field (blue line).

Flux ropes in *Cluster* observations are examined to show, for the first time, that the correlation between the core field Bcore and the IMF By depends on the guide field Bg. For large guide fields, the Bcore is found to correlate with the IMF By. However, for weak guide fields it is shown that the core fields have either a positive or negative polarity, irrespective of the IMF By. Here it is shown that spacecraft located at different hemispheres observed different polarity of the core field. This result indicates that for weak guide field reconnection the core

field generation of the magnetotail flux rope is not governed by the external IMF By. For weak guide field reconnection the flux ropes can have a significant core field whose polarity agrees with the ambient quadrupole Hall field (Fig. 18).

Magnetotail Dipolarization Fronts: Magnetotail dipolarization fronts (DF), which show a turning of the magnetic field from mainly horizontal to more vertical, are a key ingredient of magnetotail flux transport by newly reconnected closed fields. Generally DFs are accompanied with bursty bulk flows (BBFs) and are thin boundaries, separating the energetic and tenuous plasma of BBFs from that of the ambient plasma sheet.

A statistical study of the ion density and temperature variations across DFs has been performed, using nine years of *Cluster* data. Earlier studies concluded that on average the temperature increases while the density decreases across the DF. The results of this study show that ~54% of the DFs follow this pattern (type A, see Fig. 19), whereas for ~28% the temperature decreases while the density increases (type B).

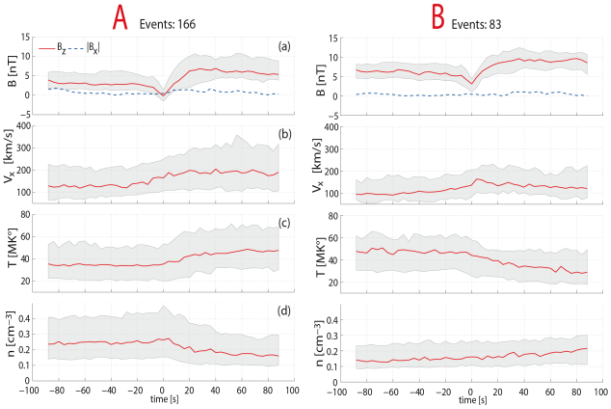

Fig. 19: Superposed Epoch analysis of (a) the B_x (dashed blue line) and B_z (solid red line) variations, (b) the X-component of the ion velocity, (c) the ion temperature, and (d) the ion density.

The main results obtained from this study are: (1) Types are independent from DF crossing location and/or the observation position in the tail; (2) Type A-flows are faster than B-flows; (3) Type B-flows are directed perpendicular to the cross-tail current in the near-Earth current sheet while type A-flows are tilted slightly duskward; (4) The background B_z of type B is higher than that of type A. These results suggest that after reconnection takes place, a BBF emerges with type A characteristics. Traveling earthward, which is in a more dipolarized region with slower plasma flow (closer to the flow braking region), it further evolves into type B.

Period and damping factor of Pi2 pulsations during oscillatory flow braking in the magnetotail: 25 observations of damped oscillatory flows in the near-Earth plasma sheet by the *THEMIS* probes during the 2008-2009 magnetotail seasons were used to compare the oscillation period and the damping factor of the plasma sheet flows with those of the Pi2 magnetic pulsations on the ground at auroral and midlatitudes near the local time of the conjugate ionospheric *THEMIS* footprints.

Whereas the dampings of the plasma sheet flows and of the pulsations on the ground occur on the same time scales, the frequency of the ground pulsations is on average twice the frequency of the plasma sheet flows. The correlation of periods (τ) and damping factors (α, Fig. 20) indicates that larger-amplitude ground pulsations at auroral latitudes are caused by the oscillatory flow braking in the plasma sheet, presumably through alternating field-aligned currents.

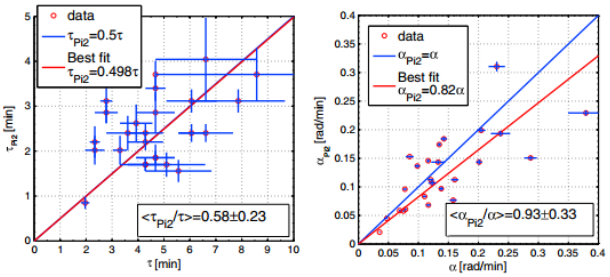

Fig. 20: Scatterplot of τ_{Pi2} against τ and α_{Pi2} against α with confidence bounds. Linear best fit is shown in red, assuming linear dependencies starting from (0,0).

Low-altitude observations of flow bursts: Coupling processes between the magnetosphere and the ionosphere are important to clarify the dissipation of the plasma sheet fast flows.

At 1000 UT on 25 February 2008, *Cluster 1* (C1) crossed the near-midnight auroral zone, at about 2 R_E altitude, while *THEMIS* THD and THE observed multiple flow bursts on the near-conjugate plasma sheet field lines. Coinciding in time with the flow bursts, C1 observed bursts of counter-streaming low-energy electrons accompanied by short time scale magnetic field disturbances embedded in flow-associated field-aligned current systems as shown in Fig. 21.

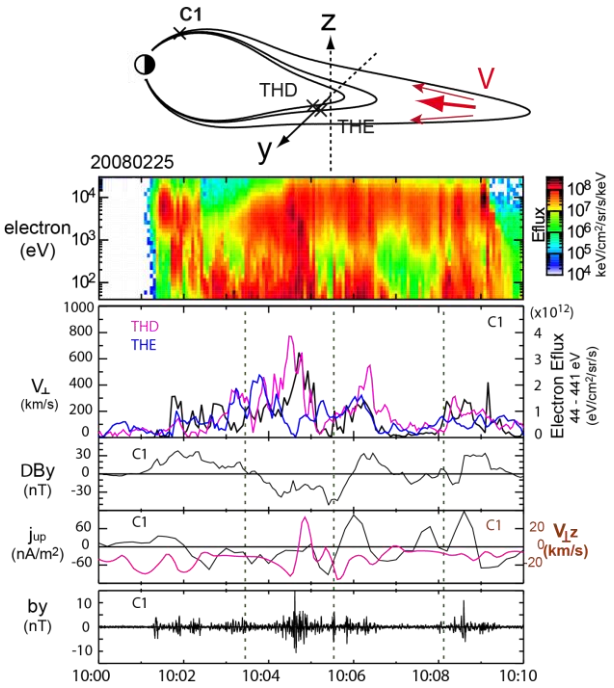

Fig. 21: Near-conjugate observations by C1, THD, THE during high-speed flow bursts as illustrated in the top. Electron energy spectra from C1; low-energy (44-441 eV) electron energy flux from C1 and flow speeds observed by THD and THE; dawn-to-dusk magnetic field disturbance and upward field-aligned current (black line) and northward flow component perpendicular to the magnetic field (red) from C1; and magnetic field disturbance (0.2-10 Hz) from top to bottom panels. Vertical lines show event start-times.

This unique conjugate event not only confirms the idea that the plasma sheet flows are the driver of the kinetic Alfvén waves accelerating the low-energy electrons but is a unique observation of disturbances in the high-altitude auroral region relevant to the multiple plasma sheet flows.

Windsock memory conditioned RAM pressure – forced reconnection in the magnetotail: Reconnection is a key physical process explaining the addition of magnetic flux to the magnetotail and the back motion of the closed flux lines to the dayside magnetosphere. This scenario or its numerous modifications can explain many aspects of solar wind-magnetosphere interaction processes, including substorms. An alternative model for the forced response was proposed, in which tail reconnection is triggered by combination of the large-scale windsock motions exhibiting memory effects and solar wind dynamic ram pressure actions on the nightside magnetopause (see Fig. 22). The windsock associated vertical ram pressure asymmetry leads to oppositely oriented motions of different parts of the tail, which can drive current sheet thinning and reconnection even during northward oriented IMF.

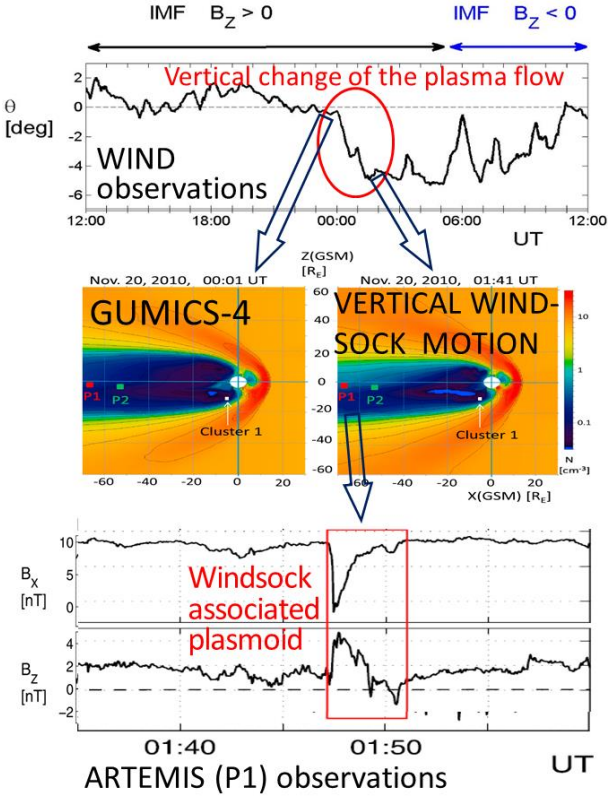

Fig. 22: Top: Directional change of the bulk flow in the solar wind; Middle: GUMICS-4 simulations of the magnetotail response; solar wind data measured by WIND are used as input; Bottom: Magnetic signatures of windsock associated plasmoid observed by ARTEMIS in the tail.

Solar System

IWF is engaged in many missions, experiments and corresponding data analysis addressing solar system phenomena. The physics of the Sun and the solar wind, its interaction with solar system bodies, and various kinds of planetary atmosphere/surface interactions are under investigation.

Sun & Solar Wind

The Sun's electromagnetic radiation, magnetic activity, and the solar wind are strong drivers for various processes in the solar system.

Solar Orbiter

Solar Orbiter is a future ESA space mission to investigate the Sun, scheduled for launch in 2017. Flying a novel trajectory, with partial Sun-spacecraft corotation, the mission plans to investigate in-situ plasma properties of the near solar heliosphere and to observe the Sun's magnetized atmosphere and polar regions. IWF builds the digital processing unit (DPU) for the *Radio and Plasma Waves (RPW)* instrument onboard *Solar Orbiter* and has calibrated the *RPW* antennas, using numerical analysis and anechoic chamber measurements. Furthermore, the institute contributes to the magnetometer.

Radio and Plasma Waves (RPW): *RPW* will measure the magnetic and electric fields at high time resolution and will determine the characteristics of the magnetic and electrostatic waves in the solar wind from almost DC to 20 MHz. Besides the 5 m long antennas and the AC magnetic field sensors, the instrument consists of four analyzers: the thermal noise and high frequency receiver; the time domain sampler; the low frequency receiver; and the bias unit for the antennas. The control of all analyzers and the communication will be performed by the DPU. IWF is responsible for the design of the DPU hardware and the boot software. The DPU board has been redesigned. The main task was the optimization of the printed circuit board in terms of electro-magnetic compatibility. A new model was built, tested and delivered to the French partners. Tests at CNES, performed end 2014, have confirmed the compliance of the new design with the EMC requirements. Because of technical problems with the antenna system and other units, the model philosophy has been changed to a proto-flight approach.

Physics

Space-time structure of solar wind turbulence: Random fluctuations in the plasma and the magnetic field in the solar wind are considered to be in a fully-developed turbulence state. The question if the fluctuation energy is anisotropically distributed remains one of the outstanding, unsolved problems in plasma turbulence. Various hypotheses exist to explain the possible turbulence anisotropy in the solar wind.

The magnetic energy spectra in the three-dimensional wave vector domain were determined observationally using the *Cluster* magnetometer data in the solar wind (Fig. 23). The spectral study provides for the first time evidence that the wave vector anisotropy is controlled by the plasma beta, the ratio of thermal to magnetic pressure. Wave vector anisotropy is characterized by an extension of the energy spectrum in the direction perpendicular to the large-scale magnetic field. The spectrum is

found to be strongly anisotropic at lower values of beta (cold plasmas), and becomes more isotropic at higher values of beta (hot plasmas). With the discovery of wave vector anisotropy, the long-standing filamentation hypothesis in plasma turbulence has successfully been confirmed by in situ observations.

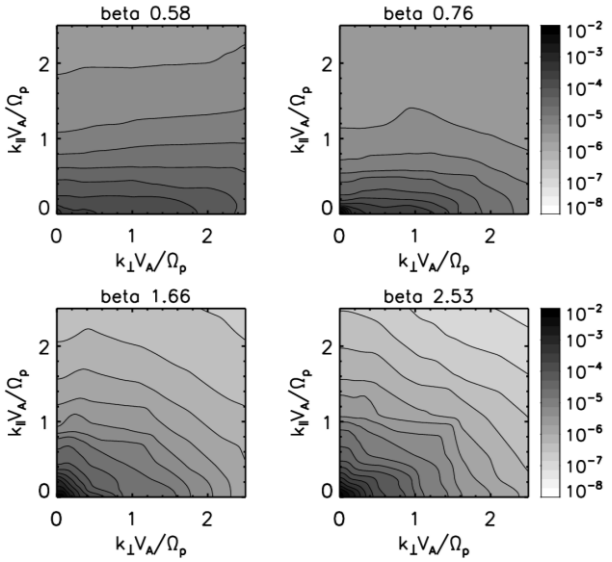

Fig. 23: Energy spectra of magnetic field fluctuations in the solar wind in a reduced two-dimensional wave vector domain. The spectrum is highly anisotropic for low-beta plasmas, and only moderately anisotropic for high-beta plasmas.

Structure and propagation of coronal mass ejections: The evolution of coronal mass ejections (CMEs) in interplanetary space is still not well understood. Interactions with solar wind structures like high-speed solar wind streams, co-rotating interaction regions or even other CMEs may alter their overall structure and lead to a deformation of their shape. This can make accurate forecasting of arrival times at Earth much more difficult. The evolution of a CME on 7 March 2012 was studied using a broad set of observations from different locations in the inner heliosphere. The CME was remotely observed by *STEREO*, and in situ measured by *MESSENGER*, *Venus Express*, *Wind* near Earth and *Mars Express*. This outstanding number of in situ detections and the stereoscopic view provided by the two *STEREO* spacecraft showed a strongly asymmetric evolution of the CME, which is illustrated in Fig. 24. The observations can be explained by a preconditioning of the background solar wind due to other CMEs.

For forecasting the possibly detrimental effects of CMEs at Earth, such as blackouts and satellite failures, parameters such as speed, magnetic field and arrival time need to be derived from remote images as accurately as possible. A study was undertaken to test the prediction of CMEs based on heliospheric images of the solar wind, which was the first to do so with a statistically significant dataset. The CME arrival at Earth was predicted to occur within about eight hours of the observed arrival, significantly improving previous approaches.

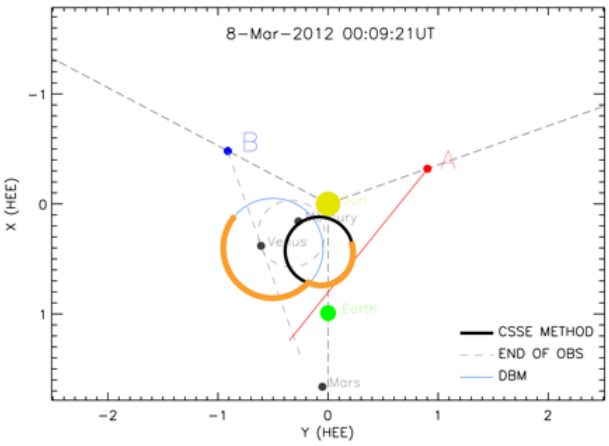

Fig. 24: Evolution of the frontal shape of the CME during propagation in the inner heliosphere. The orange curves symbolize the reconstructed asymmetric overall shape of the CME.

Flux tube instabilities and reconnection generated turbulence in the solar wind: Magnetic flux tubes represent basic structures on the Sun and in the solar wind. Flux tubes of solar origin can be magnetically twisted at photospheric, chromospheric or coronal levels and transported into interplanetary space. Twisted or untwisted flux tubes can also be generated by impulsive magnetic reconnection in the solar wind. Flux tube instabilities, such as the Kelvin-Helmholtz and the kink instabilities, may significantly contribute to the local generation of turbulence, reconnection and dissipation. The associated "fresh" turbulence may

change the field and plasma conditions supporting different local dissipation mechanisms at their characteristic wave numbers.

Recent analytical and numerical calculations show that twisted tubes moving in twisted external magnetic fields are Kelvin-Helmholtz unstable even for sub-Alfvénic motions (Fig. 25). Moving tubes with strong twists are more unstable against the kink instability than untwisted tubes. Since twisted flux tubes are frequently observed on the Sun and in the solar wind their impact on reconnection, turbulent heating and dissipation can be very important.

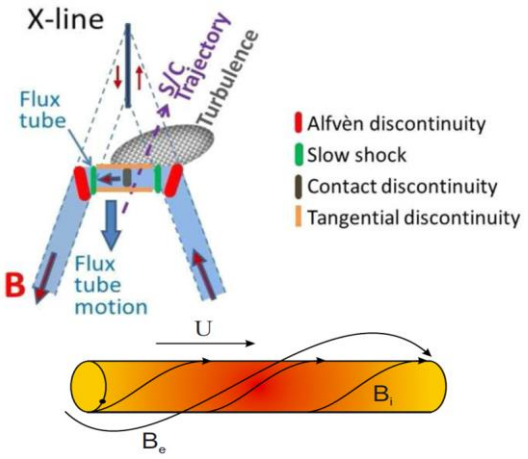

Fig. 25: Top: The structure of impulsive reconnection outflow with embedded Kelvin-Helmholtz unstable flux tube (tangential discontinuity) and turbulence; bottom: A twisted flux tube moving with speed U embedded into twisted external magnetic field.

Visibility of solar Type III radio bursts: A stereoscopic technique has been applied to localize the Type III burst source region. Observations of *Ulysses URAP*, *Cassini RPWS,* and *Wind WAVES* experiments show that the electron beam is along the interplanetary magnetic field and that the trajectory is an Archimedean spiral. This allows inferring the visibility of the source location with regard to the spacecraft position.

Mercury

Mercury is now in the center of attention because of the current NASA *Messenger* mission and the upcoming ESA/JAXA *BepiColombo* mission. The planet has a weak intrinsic magnetic field and a mini-magnetosphere, which strongly interacts with the solar wind.

BepiColombo

Two spacecraft, to be launched in early 2017, will simultaneously explore Mercury and its environment: the Japanese *Magnetospheric (MMO)* and ESA's *Planetary Orbiter (MPO)*. IWF plays a major role in developing the magnetometers for this mission: it is leading the magnetometer investigation aboard the *MMO (MERMAG-M)* and is responsible for the overall technical management of the *MPO* magnetometer *(MERMAG-P)*. For *MPO*, IWF also leads the development of *PICAM,* an ion mass spectrometer with imaging capability, which is part of the *SERENA* instrument suite, to explore the composition, structure, and dynamics of the exo-ionosphere.

During 2014, the instrument teams at IWF supported system level testing of both *MMO* and *MPO* spacecraft in Japan and Europe, respectively. It included detailed functional, vibration, and thermal tests. Furthermore, the IWF magnetometer group has started with the assembly of the *MERMAG-P* spare model.

Fig. 26: Moving BepiColombo MPO into ESA's space simulator end of October 2014 (Credits: ESA/A. Le'Floch).

In November 2014 the system level thermal vacuum and thermal balance test of the *MPO* satellite took place at ESA, which was one of the major milestones towards a successful launch of *BepiColombo* (Fig. 26).

Beside the system level tests with the qualification model, for *PICAM* the main task in 2014 was the flight model campaign. Integration of the mechanical parts was carried out in the first quarter of the year, followed by the full assembly of the instrument and initial performance tests. The tests showed the necessity of further improvements of the electronics' thermal behavior. The updates, which became available in autumn, were assembled in the final flight configuration of the sensor. *PICAM* was then verified with respect to vibration, thermal vacuum, electromagnetic cleanliness and physical properties. Consequently the unit was provisionally accepted in its pre-shipment review at the end of 2014 with the final performance verification and calibration still ongoing.

Venus & Mars

Two terrestrial planets are located just inside, Venus at 0.7 AU (AU = Astronomical Unit, distance Earth-Sun), and just outside, Mars at 1.5 AU, of the Earth's orbit around the Sun. Venus has a radius only slightly smaller than Earth and is differentiated; it does, however, not exhibit an internal magnetic field. Mars has a radius about half as big as that of the Earth, is also differentiated, but only exhibits remnant surface magnetization of a now defunct internal dynamo. Venus is characterized by a very dense atmosphere, whereas Mars has a very tenuous one. Both planets generate a so-called induced magnetosphere by their interaction with the solar wind.

Venus Express

ESA's first mission to Venus was launched in 2005. IWF takes the lead on one of the seven payload instruments, the magnetometer *VEXMAG*, which measures the magnetic field vector with a cadence of 128 Hz. It maps the magnetic properties in the magnetosheath, the magnetic barrier, the ionosphere, and the magnetotail.

Since its arrival at Venus in 2006, *Venus Express* had been on an elliptical 24-hour orbit, with a pericenter of 250 km over the north pole. After more than eight years of continuing operation well beyond the initial expectations of the mission, the mission's team initiated the aerobraking campaign right after the end of normal science operations on 18 May. During the aerobraking campaign, which lasted from May to June, the spacecraft gradually decreased its pericenter down to 130 km. The magnetometer remained ON and interesting data were collected.

However, full contact with *Venus Express* was lost on 28 November. Since then the telemetry and telecommand links had been partially reestablished, but they were very unstable and only limited information could be retrieved. All information indicated that the spacecraft was running out of propellant. Without propellant, it was no longer possible to control the attitude and orient *Venus Express* towards Earth to maintain communications. On 27 November 2014, the last magnetometer data were collected. In December, ESA officially announced the end of the *Venus Express* mission.

InSight

NASA's *InSight* mission to Mars is due for launch in 2016. IWF is contributing to the *HP³* (mole) experiment. One of the tasks of *HP³* is to explore the mechanical properties of the Martian soil as the mole penetrates the ground to a planned depth of about 3 m. In order to evaluate soil-mechanical parameters from a measured depth-versus-time curve, a model based on the theory of pile driving has been developed. This model predicts the depth progress of the mole caused by each hammer stroke as well as the vibrations of the mole and the surrounding soil. As a typical result, Fig. 27 shows the progress of the mole in different gravity environments caused by one hammer stroke.

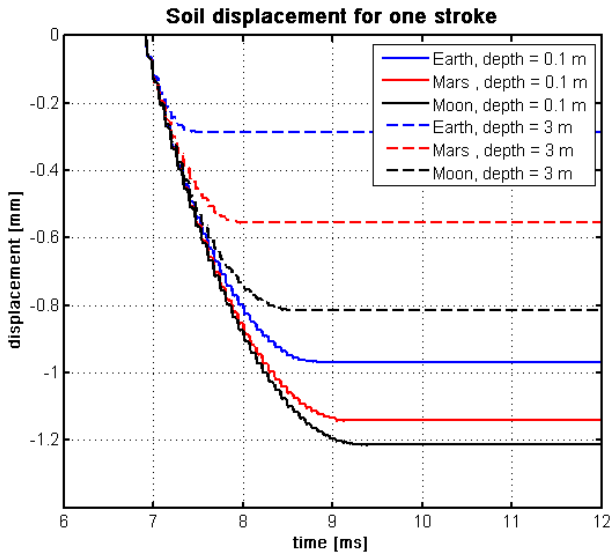

Fig. 27: Penetration of the InSight/HP³ mole into a granular regolith ground. The graphs show the permanent displacement of the mole tip caused by one hammer stroke in different gravity environments and at different depths.

Physics

The solar wind interacts directly with the atmosphere of Venus in contrast to the situation at the Earth whose magnetic field protects the upper atmosphere. Still Venus' atmosphere is partially shielded by an induced magnetic field and it needs to be understood how effective that shield is. It is expected that the effectiveness varies with solar activity but current understanding of the solar wind interaction with Venus is derived from measurements at solar maximum only. *Venus Express*, with improved instrumentation, a different orbital trajectory, and observations at solar minimum, enables understanding the evolution of the Venus atmosphere caused by the solar wind interaction.

Loss of hot C and O atoms from Mars: The escape of supra-thermal photochemically produced O and C atoms from the present Martian atmosphere during low and high solar activity has been studied with a Monte-Carlo model. The model includes (a) the initial energy distribution of photochemically produced hot atoms, (b) elastic, inelastic, and quenching collisions between the supra-thermal atoms, and (c) the ambient cooler neutral atmosphere. It applies energy dependent total and differential cross sections for the determination of the collision probability and the scattering angles. Fig. 28 shows all possible production processes and rates for hot O and C atoms. The loss rates of hot O atoms of 2.3–2.9 $\times$ 10^{25} s^{-1} indicate that the main sources of the hot O atoms are mainly related to dissociative recombination of O_2^+ and CO_2^+. The total loss rates of carbon are found to be 0.8–3.2 $\times$ 10^{24} s^{-1} for low and high solar activity, respectively, with photo-dissociation of CO being the main source. It is also found that depending on solar activity, the obtained carbon loss rates are up to 40 times higher compared to the CO_2^+ ion loss rate estimated from *Mars Express ASPERA-3* observations.

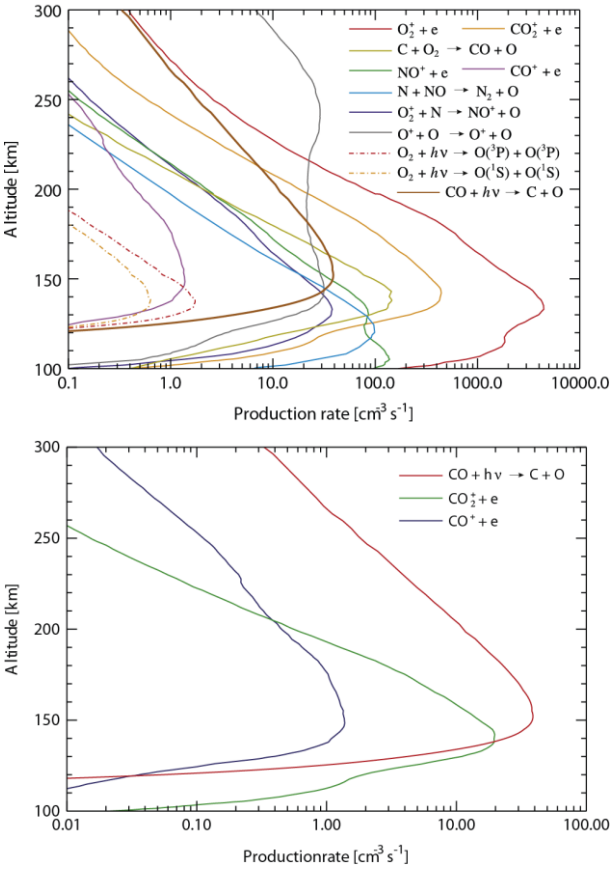

Fig. 28: Production rates of hot O atoms (top) and hot C atoms (bottom) for high solar activity.

Jupiter & Saturn

Jupiter and Saturn are the two largest planets in the solar system. Because of their atmospheric composition they are called "gas giants". Both planets rotate rapidly (approximately with

a 10 hours period) and are strongly magnetized, with the Jovian multipole field tilted at 10° and the Kronian field almost dipolar and perfectly aligned with the rotational axis. The magnetospheres are dominated by internal plasma sources, generated by the large number of moons, particularly Io at Jupiter and Enceladus at Saturn. The gas giants are also strong sources of radio emissions.

Cassini

In 2014 the 10th anniversary of the *Cassini* Saturn orbit insertion was celebrated. *Cassini* has provided much new understanding about the Saturnian system, and it will continue to do so until September 2017, when the spacecraft will make its deadly plunge into Saturn's atmosphere. IWF participated in *Cassini* with the *Radio and Plasma Wave Science (RPWS)* instrument.

JUICE

ESA's first Large-class mission *JUpiter ICy moons Explorer (JUICE)* is planned for launch in 2022 and arrival at Jupiter in 2030. It will spend at least three years making detailed observations of the giant gaseous planet Jupiter and three of its largest moons, Ganymede, Callisto and Europa. IWF is taking part with Co-I-ship for three different selected instrument packages.

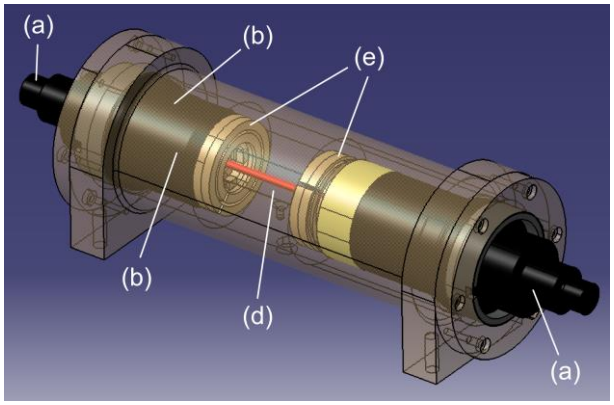

Fig. 29: 3D model of the CDSM sensor with two fibre couplers (a), a polarizer (b), a quarter-wave plate (c), a 25 mm long Rb-filled glass cell (d) mounted between two damping elements (e) and the sensor housing.

For the *Jupiter Magnetic Field Package (J-MAG)* IWF supplies an atomic scalar sensor (Fig. 29), which is developed in collaboration with TU Graz. It was only defined as optional after instrument selection but became a baseline sensor with the completion of the Preliminary Science Requirements Review process in May 2014.

The *Particle Environment Package (PEP)* is a plasma package with sensors to characterize the plasma environment in the Jovian system and the composition of the exospheres of Callisto, Ganymede, and Europa. IWF participates in the *PEP* consortium on Co-I basis in the scientific studies related to the plasma interaction and exosphere formation of the Jovian satellites.

Last but not least, IWF is responsible for the antenna calibration of the *Radio and Plasma Wave Investigation (RPWI)* instrument. Numerical simulations of the antenna reception properties for the *RPWI* instrument have led to a changed baseline configuration regarding the antennas, which should be placed as an antenna triad onto the magnetometer boom.

Physics

Remote sensing of the Io torus plasma ribbon: Jovian hectometric (HOM) emissions were recorded by the *Cassini/RPWS* experiment during its Jupiter flyby. Intensity extinction of HOM radiation was observed and interpreted as a refraction effect occurring inside the Io plasma torus. This lead to an estimation of the electron density and showed that UV and HOM wavelength observations have common features related to the morphology of the Io plasma torus. Maxima of enhancements/attenuations of UV/HOM observations occur close to the longitudes of south and north magnetic pole.

Saturn kilometric radiation and the Great White Spot: The periodicity of Saturn kilometric radiation (SKR), a strong auroral radio emission in the frequency range from a few kHz to

1.2 MHz, is varying with time over the years as can be seen in Fig. 30. Before Saturn equinox in August 2009 the SKR modulation spectrogram shows two different periods for SKR radiated from the northern (~10.6 h) and southern (~10.8 h) hemisphere.

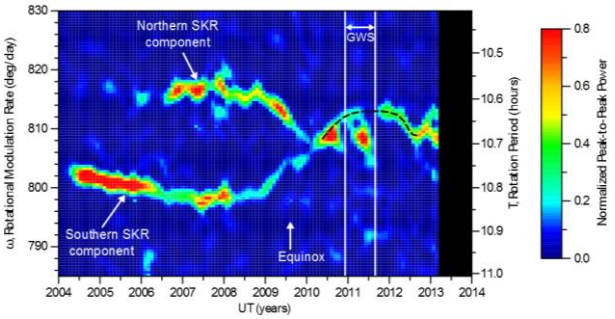

Fig. 30: Rotational modulation of SKR as a function of time from 2004 until early 2013. There are two periods related to SKR from different hemispheres until shortly after equinox, but there is mainly one period until 2013 (black dashed line) except for a few month in early 2011. The duration of the Great White Spot (GWS), contemporaneous to a remarkable feature in the spectrogram, is indicated by vertical white lines.

The Great White Spot (GWS) was a giant thunderstorm that raged in Saturn's atmosphere from December 2010 until August 2011. It is exactly during this time that the SKR modulation period experienced a sharp drop and a sudden jump back to a faster rotation. This relation is supporting the theory that Saturn's magnetospheric periodicities are driven by the planet's upper atmosphere. The GWS was a source of intense gravity waves that may have caused a global change in Saturn's thermospheric winds via energy and momentum deposition. Hence, a change of winds in the auroral thermosphere can influence the slippage of the magnetosphere via field-aligned currents, which generate the SKR.

Comets

Space missions like *Giotto*, *VEGA*, *Stardust*, *Deep Impact*, and others have dramatically increased our knowledge on comets and their nuclei from fast flybys. *Rosetta*'s arrival at comet 67P/Churyumov-Gerasimenko (67P/CG) in August 2014 and the landing of *Philae* on the comet's surface in November changes the field of cometary physics completely.

Rosetta

ESA's *Rosetta* arrived at 67P/CG after a ten year journey through interplanetary space. As solar panels are the only energy source for the spacecraft, which do not supply enough energy around *Rosetta's* aphelion the craft was put into sleeping mode in June 2011. After a successful wake-up call in January 2014, the commissioning phase for the instruments started, testing all the instruments before arrival. *Rosetta* arrived at the comet on 6 August. After extensive surface mapping, the *Philae* lander was dropped onto the comet's nucleus on 12 November. *Rosetta* will continue to follow 67P/CG along its orbit through perihelion and beyond, at least until mid 2016. *Philae* has used the power in its batteries during the first science period of approximately 30 hours, and is now recharging.

IWF participates in five instruments aboard both orbiter and lander and is working now on the evaluation and interpretation of the data.

MIDAS: The *MIDAS* instrument on-board the *Rosetta* orbiter, led by IWF, is designed to collect and analyze the smallest dust particles ejected from comet 67P/CG. By using the technique of atomic force microscopy, *MIDAS* builds 3D images of dust grains with nanometer resolution. These can be used to address fundamental questions about the building blocks of comets and our Solar System.

Since wake-up *MIDAS* has performed nearly 400 scans. Initial results show that the comet emits fewer small particles than expected, but this may change as 67P/CG becomes more active.

MUPUS (Multi-Purpose Sensor): After landing of the *Philae* spacecraft on comet 67P/CG on 12 November 2014 the penetrator of the *MUPUS* experiment was deployed and made an attempt to hammer itself into the cometary surface. The

hammering device performed about 500 hammer strokes, most of them with the maximum possible power. However, after having moved through a very soft dust layer with a thickness of several cm, it encountered a very hard layer, with an estimated crushing strength in the range of several MPa, which the *MUPUS-PEN* instrument was not able to penetrate. This hard layer consists supposedly of sintered water ice formed by the interaction of the original cometary material with the solar radiation during many encounters of the comet with the Sun. Similar ice crusts were observed almost 20 years ago in laboratory experiments devoted to the "simulation" of cometary surface processes.

Although the *MUPUS* instrument could not perform the planned thermal conductivity measurements during the first science sequence, its thermal sensors nevertheless performed valuable temperature measurements, which are currently being evaluated. The temperatures measured by the sensors installed inside the *MUPUS-PEN* tube before and after its deployment are shown in Fig. 31.

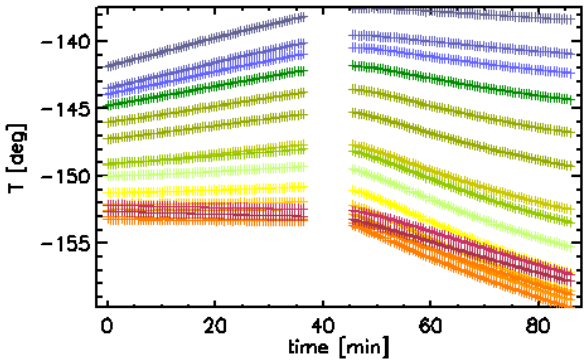

Fig. 31: Temperature trend measured by the MUPUS-PEN sensors before and after the deployment of the instrument at the cometary surface.

The decreasing temperature trend after the deployment can be interpreted either as increased radiation cooling or that the penetrator has moved into a cold dust pile or layer. There is still some hope that, after the comet has come closer to the Sun by about May/June 2015, the lander and its experiments will be able to perform further measurements in the frame of the planned LTS (Long Term Science) phase.

Physics

Field line draping and mirror modes at comet 1P/Halley: In preparation for the *Rosetta* mission the data from the comet 1P/Halley flybys by *Vega 1, 2* and *Giotto* were investigated for two characteristic phenomena: mirror mode waves (MMW) and field line draping. Both are created by the interaction of the solar wind magnetoplasma with the outgassing comet. The gas from the comet gets ionized by solar UV radiation or by collisions. The ions get picked up by the solar wind magnetic field and create a conducting layer around the comet. The solar wind magnetic field cannot pass unhindered though this layer and gets "hung-up"; the field lines go slower near the comet then farther away and drape themselves around it. It is shown that there is a linear dependence between the sun-comet direction (Bx) of the field and the radially-from-the-comet component (Brad) for draping (see Fig. 32). Intervals of draping and non-draping alternate (are nested) in the magnetic pile-up region. Comparing the draping between the three flybys shows that it can change significantly over the timespan of eight days.

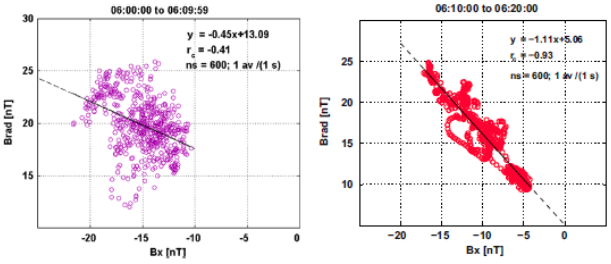

Fig. 32: Scatterplot of Brad vs. Bx for an interval of non-draping (left) and an interval of draping (right).

Unlike in planetary magnetosheaths, it was shown that for comets MMWs are not generated at the bowshock and transported down stream, but are generated near the comet. The freshly picked-up ions create a ring distribution in phase space, which is unstable for the generation of these waves. Their size was es-

tablished to be about 2 ion (H_2O) gyro radii. The upstream solar wind conditions and the comet's gas production rate plays a strong role in the occurrence rate of MMWs, which becomes clear after comparing the three Halley flybys.

Exoplanets

The field of exoplanet (i.e. planets around stars other than our Sun) research has developed strongly, in the past decade. Since the discovery of 51 Peg b, the first Jupiter-type gas giant outside our Solar System, more than 1000 exoplanets, about 800 planetary systems with more than 170 multiple planet systems have been detected. Better observational methods have led to the finding of so-called super-Earths, some of them even inside the habitable zones of their host stars. However, the majority of super-Earths have low average densities, which indicate that they are surrounded by dense hydrogen envelopes or volatiles. By minimizing the uncertainties of the radii with the upcoming missions *CHEOPS* and *PLATO*, densities and hence the structure of these planets will be better determined.

CHEOPS

ESA's first Small-class mission *CHEOPS (CHaracterizing ExOPlanets Satellite,* Fig. 33) will be the first space mission dedicated to characterize exoplanets in detail. It will focus on exoplanets with typical sizes ranging from Neptune down to Earth diameters orbiting bright stars. This mission will also try to specify the components of their atmospheres.

The electrical subsystem for *CHEOPS* consists of two units, the BEE (Back-End-Electronics) and the camera. IWF is responsible for the development of the fully redundant *BEE.* The institute develops the DPU (digital processing unit) and its boot software, while the PSU (power supply unit) is a contribution of RUAG Space Austria. The BEE provides the electrical interface to the spacecraft and performs the control of the *CHEOPS* instrument. Commands are routed from the spacecraft through the BEE to the camera and the image data are compressed and packetized for transmission.

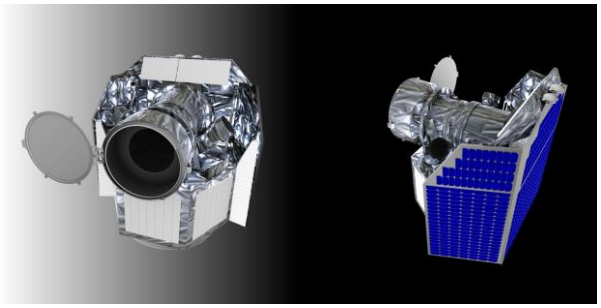

Fig. 33: 3D model of the CHEOPS spacecraft.

EADS-CASA was selected as the spacecraft provider by ESA in April 2014. This was the starting point to establish the final requirement specification for the BEE electronics. A statement of work for the industrial PRODEX contract for the PSU has been established. The development of the processor board started with a prototype, which shall be ready in the first quarter 2015. The documentation for the preliminary design review has been prepared. In parallel, the specifications for the boot software have been established. The release of the first version is planned for mid-2015.

Physics

Exoplanet magnetic fields and mass loss: To study the effects of intrinsic magnetic fields of hydrodynamically expanding, partly ionized upper atmospheres of giant exoplanets in close-orbit locations on atmospheric escape processes, a hydrodynamic model was applied to HD 209458b. The major focus of this study was the self-consistent inclusion of radiative heating and ionization of the expanding atmospheric gas in the host star's radiation environment. Primary attention was paid to investigation of the role of specific inner and outer boundary conditions, under which different regimes of escaping gas (free- and restricted-flow) are formed. A comparative study of different processes, such as XUV heating, ionization and recombination, IR-cooling, adi-

abatic and Lyman-α cooling, as well as Lyman-α reabsorption has been carried out. It was found that under the typical conditions of an orbital distance 0.05 AU around a Sun-type star a Hot Jupiter plasma envelope may reach maximum temperatures up to 9000 K with a hydrodynamic escape speed of about 9 km/s resulting in the mass loss rates of (4-7) x 10^{10} g/s. In the range of considered stellar-planetary parameters and XUV fluxes that is close to the mass loss in the energy limited case. Fig. 34 illustrates the calculated profiles.

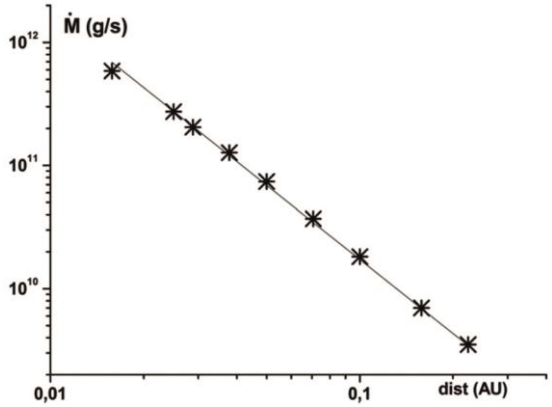

Fig. 34: Stellar XUV induced mass loss rate dependence as a function of orbital distance of HD 209458b to a Sun-like host star.

Transit observations of the studied exoplanet in the stellar Ly-α line revealed a strong absorption in the blue and red wings of the line that can be interpreted as H atoms escaping from the planet's exosphere at high velocities. The following sources for the absorption were suggested: acceleration by the stellar radiation pressure; natural spectral line broadening; or charge exchange with the stellar wind around an exoplanet magnetic obstacle. The transit observation of the Hubble Space Telescope can be reproduced by a model that includes all aforementioned processes. The results support a stellar wind with a velocity of 400 km/s at the time of the observation and a planetary magnetic moment of 1.6 × 10^{26} A/m². Fig. 35 illustrates the corresponding Lyman-α absorption in comparison to the transit observation by the Hubble Space Telescope.

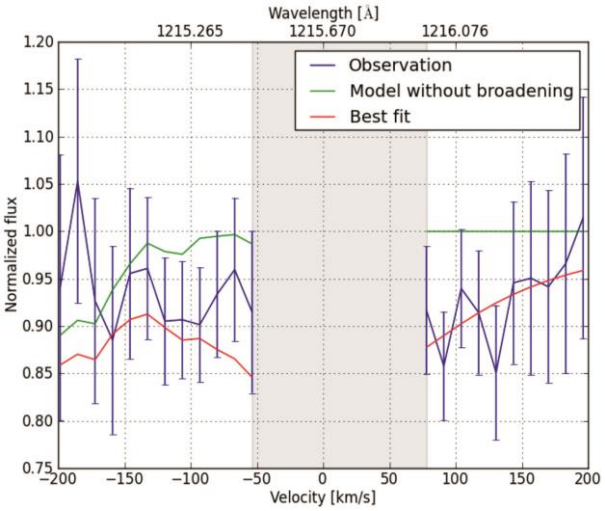

Fig. 35: Comparison of modeled (red line, including spectral broadening; green line, without spectral broadening) and observed (blue line) Ly-alpha spectra at mid-transit. The region of contamination by geocoronal emission at low velocities is excluded and marked by the shaded area.

The capture and loss of primordial hydrogen atmospheres has been also investigated for rocky protoplanets inside the habitable zone of Sun-like stars with masses between 0.1 and 5 M_E during the first 100 Myr of planetary evolution. The evolving stellar activity and changing radiation in the XUV range was taken into account, and the masses of collected atmosphere envelopes of nebula origin have been calculated. It is shown that for the typical evolution of a G star, the cores with masses below 2 M_E can evolve to planets with terrestrial-type secondary atmospheres, while more massive cores stay as Mini-Neptunes surrounded by a thick hydrogen-helium envelope during their whole life times.

Testing & Manufacturing

Instruments onboard spacecraft are exposed to harsh environments, e.g., vacuum, large temperature ranges, radiation and high mechanical loads during launch. Furthermore, these instruments are expected to be highly reliable, providing full functionality over the entire mission time, which could last for even more than a decade.

Vacuum Chambers

The *Small Vacuum Chamber* is a manually controlled, cylindrical vacuum chamber (160 mm diameter, 300 mm length) for small electronic components or printed circuit boards. It features a turbo molecular pump and a rotary dry scroll forepump. A pressure level of 10^{-10} mbar can be achieved.

The *Medium Vacuum Chamber* has a cylindrical stainless steel body with the overall length of 850 mm and a diameter of 700 mm. A dry scroll forepump and a turbo molecular pump provide a pressure level of about 10^{-7} mbar. A target manipulator with two axes and an ion beam source are installed. This chamber mainly serves for functional tests of the ion mass spectrometer for *BepiColombo*.

The *Large Vacuum Chamber* has a horizontal cylindrical stainless steel body and door, a vision panel, two turbo molecular pumps and a dry scroll forepump. A pressure of 10^{-7} mbar can be achieved. The cylinder has a diameter of 650 mm and a length of 1650 mm. During shutdown the chamber is vented with nitrogen. A target manipulator inside the chamber allows for computer-controlled rotation of the target around three mutually independent perpendicular axes. The vacuum chamber is enclosed by a permalloy layer for magnetic shielding. To enable the baking of structures and components (to outgas volatile products and unwanted contaminations), the chamber is equipped with a heater around the circumference.

The *Thermal Vacuum Chamber* is fitted with two turbo molecular pumps, a dry scroll forepump, and an ion getter pump, which together achieve a pressure level of 10^{-6} mbar and allow quick change of components or devices to be tested. A thermal plate installed in the chamber and liquid nitrogen are used for thermal cycling in a temperature range between −90 °C and +140 °C. The vertically oriented cylindrical chamber allows a maximum experiment diameter of 410 mm and a maximum height of 320 mm.

The *Surface Laboratory Chamber* is dedicated to surface science research. It has a diameter of 400 mm and a height of 400 mm, extendable up to 1200 mm. One rotary vane pump and one turbo-molecular pump achieve a minimum pressure of 10^{-5} mbar. With an external thermostat the chamber temperature can optionally be controlled between −90°C and +50°C.

The *Sample Chamber* contains an 8µ particle filter and allows measurements of grain sample electrical permittivity. One rotary vane pump achieves a minimum pressure of 10^{-3} mbar.

Other Test Facilities

The *Temperature Test Chamber* allows verifying the resistance of electronic components and circuits to most temperature conditions that occur under natural conditions, i.e., −40 °C

to +180 °C. The chamber has a test space of 190 litres and is equipped with a 32-bit control and communication system.

The *Penetrometry Test Stand* is designed to measure mechanical soil properties, like bearing strength. The *UV Exposure Facility* is capable to produce radiation between 200-400 nm (UV-A, UV-B, UV-C).

Magnetometer calibration: A three-layer magnetic shielding made from mu-metal is used for all basic magnetometer performance and calibration tests. The remaining DC field in the shielded volume is <10 nT and the remaining field noise is <2 pT/√Hz at 1 Hz. A special Helmholtz coil system allows generating field vectors of up to ±30000 nT around the sensor under test.

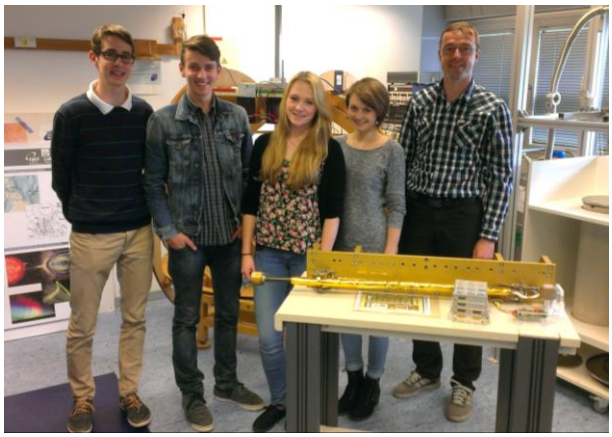

Fig. 36: Stiftsgymnasium St. Paul visiting the temperature test facility of the IWF magnetometer lab.

The *Magnetometer Temperature Test Facility* (Fig. 36) is used to test magnetic field sensors between -170 °C and +220 °C in a low field and low noise environment. Liquid nitrogen is the base substance for the regulation, which is accurate to ±0.1 °C. A magnetic field of up to ±100000 nT can be applied to the sensor during the test cycles.

Flight Hardware Production

Clean room: Class 10000 (according to U.S. Federal Standard 209e) certified laboratory with a total area of 30 m². The laboratory is used for flight hardware assembling and testing and accommodates up to six engineers.

Clean bench: The laminar flow clean bench has its own filtered air supply. It provides product protection by ensuring that the work piece in the bench is exposed only to HEPA-filtered air (HEPA = High Efficiency Particulate Air). The internal dimensions are 118 x 60 x 56 cm³.

Vapor phase and IR soldering machine: The vapor phase soldering machine is suitable for mid size volume production. The maximum board size is 340x300x80 mm³. Vapor phase soldering is currently the most flexible, simplest and most reliable method of soldering. It is ideally suited for all types of surface mounted device (SMD) components and base materials. It allows processing of all components without the need of any complicated calculations or having to maintain temperature profiles. For placing of fine pitch parts and rework of electronic boards an infrared soldering and precision placing system is used.

Outreach

Public Outreach

IWF is actively engaged in science education and public outreach. 2014 PR activities concentrated on *Rosetta*. ESA's comet chaser, launched in 2004, was put into deep-space hibernation in June 2011. On 20 January 2014 it was woken up and IWF invited the public to join this exciting moment and welcomed more than 100 visitors (Fig. 37).

Fig. 37: Children shouting "Wake up Rosetta" during the Rosetta Wake-Up event at IWF Graz.

The URANIA series of lectures in March and April were dedicated to "Cometary research in Graz", too.

In May, IWF participated in the exhibition "Wir sind Europa" during the Graz Spring Fair and presented several *Rosetta* (spacecraft and payload) models.

Finally, the general public could follow the first-ever landing on a comet on 12 November 2014 live at IWF (Fig. 38). Because of the historic significance and the enormous popular interest this was a multi-local event with gatherings at ÖAW in Vienna and a live broadcast at the Graz UCI cinema. LR Drexler, and Deputy Mayor Schröck kept their fingers crossed for Philae during the "Rosetta Touchdown" at IWF. In Vienna, Vice-President Alram welcomed BM Stöger (bmvit), FWF president Ehrenfreund as well as FFG representatives Pseiner and Posch A livestream was shown on Youtube (www.youtube.com/watch?v=p4ScjZawnac).

Throughout the rest of the year, many different groups and school classes ("SeniorInnenreferat" of the City of Graz, VS Eisteich, VS Peter Rosegger, VS Raaba, VS Ursulinen, NMS Andritz, NMS Krottendorf, and Stiftsgymnasium St. Paul) visited the institute.

From 27 February until 11 May, Universalmuseum Joanneum showed the exhibition „Idee und Form. Mathematik und die Schönheit der Kunst", which was well visited and co-curated by Bruno Besser.

Fig. 38:, IWF Vice-Director Magnes (center) welcomed LR Drexler (left) and Deputy Mayor Schröck (right) at the "Rosetta Touchdown" event (Photo: Sabine Hoffmann).

On 4 April, more than 1600 people visited both IWF and the Lustbühel Observatory during the "Lange Nacht der Forschung". The program included experiments, movie shows, guided tours through the labs, a demonstration of the laser, a remote controlled Mars Rover tour over a simulated surface of the red planet, and last

but not least a "How to cook a comet" show (Fig. 39).

Fig. 39: Children waiting to get a bit of a comet, which surprisingly tasted like chocolate icecream.

From 4–5 September, the Summer University "Graz in Space" was held at University of Graz. About 70 participants listened to several talks, which concentrated on Rosetta, space weather and possible life on exoplanets.

On 19 September, Deputy Mayor Schröck organized the first "Grazer Weltraumtag" in Graz downtown with exhibitions, experiments, computer games, children's corners, and a stage discussion (Fig. 40).

Fig. 40: Werner Magnes and Manfred Steller (from right) participated in the stage discussion moderated by Kleine Zeitung journalist Norbert Swoboda.

From 22–24 September, IWF hosted the UN/Austria Symposium on "Space Science and the United Nations" with more than 50 participants from all over the world.

From 8 October until 12 November 2014 the "Grazer ALL-Tage" presented science and art across the universe. IWF Graz opened its labs to interested young people and gave several talks in the completely overbooked UCI Annenhof cinema.

On 6 November, IWF director Wolfgang Baumjohann was invited by APA to a panel discussion about Austria's contribution to "Big Science" matters (Fig. 41).

Fig. 41: APA-Science event in Vienna with Hannes Androsch, Sabine Ladstätter, Alois Saria, Christian Müller, Wolfgang Baumjohann, Jochen Schieck, and Daniel Weselka (fltr, photo: APA/APA-Fotoservice / Schedl).

On 28 November, Daniel Schmid presented in the frame of a bmvit-organized research speed dating his work to students of the BHAK and HBLA Klagenfurt (Fig. 42).

From 1–4 December, "Post Alpach" was held at Schloss St. Martin, where Günter Kargl served as tutor.

On 4 December, the Embassy of Slovenia organized together with IWF Graz and the Pavelhaus the presentation of the book "Herman Potočnik Noordung".

In the framework of the "FEMtech" program of FFG, one young lady from KFU Graz worked at IWF for two months. During summer time, three high-school students from BRG

Monsbergergasse Graz (solar corona and its expansion into interplanetary space), HTL-BULME Graz-Gösting (design and assembly of a Spacewire time display), and Akademisches Gymnasium Graz (influence of the foreshock region on the dayside magnetopause and on geomagnetic activity), performed an internship at IWF under the "Talente-Praktika" program of FFG.

Fig. 42: Daniel Schmid explains experimental plasma physics to students (Photo: PlanSinn).

Awards & Recognition

During the EGU General Assembly, Rumi Nakamura was the first woman to be awarded the Julius Bartels Medal for her most outstanding contributions to our current understanding of solar-terrestrial relations (Fig. 43).

Meetings

From 19 to 21 May the workshop Penetrometry in the Solar System III was hosted by the institute at Seggau Castle with almost 20 international participants. The meeting was organized by Norbert Kömle and Günter Kargl.

The Annual Meeting of the Austrian Physical Society, taking place in Pöllau from 24 to 27 September with 180 participants, was co-organized by Bruno Besser.

In October Manfred Steller organized the *Cheops* Programm Meeting and *Solar Orbiter RPW* Consortium Meeting with approx. 40 participants each. Both were held at the institute.

From 4 to 6 November the *Rosetta RPC* Team Meeting was held at at Seggau Castle with almost 50 participants from all over the world. The meeting was organized by Martin Volwerk.

Wolfgang Baumjohann served as Vice Director and on the Program Committee of the Summer School Alpbach, which took place from 15 to 24 July and was dedicated to „Geophysics of the Terrestrial Planets". Every year, 60 students and about 25 lecturers and tutors from among ESA's member states are invited to this meeting.

Additionaly, H. Lammer, Y. Narita, and M. Volwerk were members of program and/or scientific organizing committees for three international conferences and/or workshops. M. Andriopoulou, M.Y. Boudjada, G. Fischer, G. Kargl, M.L. Khodachenko, G. Kirchner, H. Lammer, C. Möstl, R. Nakamura, Y. Narita, M. Volwerk, and Z. Vörös organized or chaired 21 sessions at 10 international meetings.

Fig. 43: Deputy Mayor Martina Schröck congratulated Rumi Nakamura to her Bartels Medal (Photo: Stadt Graz/Sonja Tautscher).

Lecturing

IWF members are actively engaged in teaching at three universities and two universities of applied sciences. In summer 2014 and in winter term 2014/2015 the following lectures were given:

KFU Graz

Einführung in die Aeronomie (Lammer)

Einführung in die Planetologie (Kömle)

Introduction to Geophysics and Planetary Physics (Kargl et al.)

Praktikum aus Weltraumphysik und Aeronomie (Nakamura et al.)

TU Graz

Advanced Satellite Geodesy (Baur et al.)

Design and Development of Space Qualified Hardware (Magnes)

Digitale Audiotechnik, Labor (D. Fischer, Magnes)

GGOS and Reference Systems (Baur et al.)

Signalprozessortechnik (Magnes)

Weltraumplasmaphysik (Plaschke)

TU Braunschweig

Plasma-Astrophysik (Narita)

FH Joanneum

Mathematik 1 für Informatik (Lichtenegger)

FH Wiener Neustadt

Space Environment and Interactions (D. Fischer, Plaschke)

Advanced Course

The four semesters Master Studies curriculum „Space Sciences and Earth from Space“ as a cooperative curriculum within the frame of NAWI (KFU and TU) Graz was established in 2011 and continues with starts each winter term. At present approximately 30 students have enrolled.

Theses

Besides lecturing, members of the institute are supervising Bachelor, Diploma, Master and Doctoral Theses. In 2014, the following supervised theses have been completed:

Kislyakova, K.: Modeling of the Interaction between Stellar Wind Plasma and the Upper Atmosphere of Exoplanets as a Tool for Evolution Studies, Doctoral Thesis, Universität Graz, 181 pages (2014)

Rollett, T.: Evolution of Coronal Mass Ejections and their Heliospheric Imprints, Doctoral Thesis, Universität Graz, 103 pages (2014)

Schaffer, A.: Calibration Strategy for a Thermal Probe Applicable in Planetary Research, Diploma Thesis, Universität Graz, 129 pages (2014)

Schantl, P.: Analysis of Turbulence in the Solar Wind, Diploma Thesis, Universität Graz, 104 pages (2014)

Tiefenbacher, P.: Measurements of Thermal Properties with a Dual-Needle Probe for Planetary Applications, Diploma Thesis, Universität Graz, 167 pages (2014)

Wolbang, D.: Seismo-Electromagnetic Parameter Study of Sub-Ionospheric VLF Radio Links in Europe, Diploma Thesis, Universität Graz, 118 pages (2014)

Publications

Refereed Articles

Alonso, R., C. Moutou, M. Endl, J.-M. Almenara, E.W. Guenther, M. Deleuil, A. Hatzes, S. Aigrain, M. Auvergne, A. Baglin, P. Barge, A.S. Bonomo, P. Bordé, F. Bouchy, C. Cavarroc, J. Cabrera, S. Carpano, Sz. Csizmadia, W.D. Cochran, H.J. Deeg, R.F. Díaz, R. Dvorak, A. Erikson, S. Ferraz-Mello, M. Fridlund, T. Fruth, D. Gandolfi, M. Gillon, S. Grziwa, T. Guillot, G. Hébrard, L. Jorda, A. Léger, H. Lammer, C. Lovis, P.J. MacQueen, T. Mazeh, A. Ofir, M. Ollivier, T. Pasternacki, M. Pätzold, D. Queloz, H. Rauer, D. Rouan, A. Santerne, J. Schneider, M. Tadeu dos Santos, B. Tingley, R. Titz-Weider, J. Weingrill, G. Wuchterl: Transiting exoplanets from the CoRoT space mission. XXVI. CoRoT-24: A transiting multiplanet system, *Astron. Astrophys.*, **567**, A112 (2014)

Arridge, C.S., N. Achilleos, J. Agarwal, C.B. Agnor, R. Ambrosi, N. André, S.V. Badman, K. Baines, D. Banfield, M. Barthélémym, M.M. Bisi, J. Blum, T. Bocanegra-Bahamon, B. Bonfond, C. Bracken, P. Brandt, C. Briand, C. Briois, S. Brooks, J. Castillo-Rogez, T. Cavalié, B. Christophe, A.J. Coates, G. Collinson, J.F. Cooper, M. Costa-Sitja, R. Courtin, I.A. Daglis, I. de Pater, M. Desai, D. Dirkx, M.K. Dougherty, R.W. Ebert, G. Filacchione, L.N. Fletcher, J. Fortney, I. Gerth, D. Grassi, D. Grodent, E. Grün, J. Gustin, M. Hedman, R. Helled, P. Henri, S. Hess, J.K. Hillier, M.H. Hofstadter, R. Holme, M. Horanyi, G. Hospodarsky, S. Hsu, P. Irwin, C.M. Jackman, O. Karatekin, S. Kempf, E. Khalisi, K. Konstantinidis, H. Krüger, W.S. Kurth, C. Labrianidis, V. Lainey, L.L. Lamy, M. Laneuville, D. Lucchesi, A. Luntzer, J. MacArthur, A. Maier, A. Masters, S. McKenna-Lawlor, H. Melin, A. Milillo, G. Moragas-Klostermeyer, A. Morschhauser, J.I. Moses, O. Mousis, N. Nettelmann, F.M. Neubauer, T. Nordheim, B. Noyelles, G.S. Orton, M. Owens, R. Peron, C. Plainaki, F. Postberg, N. Rambaux, K. Retherford, S. Reynaud, E. Roussos, C.T. Russell, A.M. Rymer, R. Sallantin, A. Sánchez-Lavega, O. Santolik, J. Saur, K.M. Sayanagi, P. Schenk, J. Schubert, N. Sergis, E.C. Sittler, A. Smith, F. Spahn, R. Srama, T. Stallard, V. Sterken, Z. Sternovsky, M. Tiscareno, G. Tobie, F. Tosi, M. Trieloff, D. Turrini, E.P. Turtle, S. Vinatier, R. Wilson, P. Zarka: The science case for an orbital mission to Uranus: Exploring the origins and evolution of ice giant planets, *Planet. Space Sci.*, **104**, 122-140 (2014)

Artemyev, A.V., A.P. Walsh, A.A. Petrukovich, W. Baumjohann, R. Nakamura, A.N. Fazakerley: Electron pitch angle/energy distribution in the magnetotail, *J. Geophys. Res.*, **119**, 7214-7227 (2014)

Aryan, H., M.A. Balikhin, A. Taktakishvili, T.-L. Zhang: Observation of shocks associated with CMEs in 2007, *Ann. Geophys.*, **32**, 223-230 (2014)

Baur, O., H. Bock, E. Höck, A. Jäggi, S. Krauss, T. Mayer-Gürr, T. Reubelt, C. Siemes, N. Zehentner: Comparison of GOCE-GPS gravity fields derived by different approaches, *J. Geodesy*, **88**, 959-973 (2014)

Boakes, P.D., R. Nakamura, M. Volwerk, S.E. Milan: ECLAT Cluster spacecraft magnetotail plasma region identifications (2001-2009), *Dataset Papers in Science*, **2014**, 684305 (2014)

Boudjada, M.Y., P.H.M. Galopeau, M. Maksimovic, H.O. Rucker: Visibility of Type III burst source location as inferred from stereoscopic space observations, *Adv. Radio Sci.*, **12**, 167-170 (2014)

Boudjada, M.Y., P.H.M. Galopeau, S. Sawas, H. Lammer: Remote sensing of the Io torus plasma ribbon using natural radio occultation of the Jovian radio emissions, *Ann. Geophys.*, **32**, 1119-1128 (2014)

Bourdin, P.-A.: Standard 1D solar atmosphere as initial condition for MHD simulations and switch-on effects, *Cent. Eur. Astrophys. Bull.*, **38**, 1-10 (2014)

Bourdin, Ph.-A., S. Bingert, H. Peter: Coronal loops above an active region: Observation versus model, *Publ. Astron. Soc. Japan*, **66**, 1-8 (2014)

Brockmann, J.M., N. Zehentner, E. Höck, R. Pail, I. Loth, T. Mayer-Gürr, W.-D. Schuh: EGM_TIM_RL05:

An independent geoid with centimeter accuracy purely based on the GOCE mission, *Geophys. Res. Lett.*, **41**, 8089–8099 (2014)

Chai, L., M. Fraenz, W. Wan, Z. Rong, T.-L. Zhang, Y. Wei, E. Dubinin, J. Zhong, X. Han, S. Barabash: IMF control of the location of Venusian bow shock: The effect of the magnitude of IMF component tangential to the bow shock surface, *J. Geophys. Res.*, **119**, 9464–9475 (2014)

Cheng, C.-C., I.R. Mann, W. Baumjohann: Association of consecutive Pi2–Ps6 band pulsations with earthward fast flows in the plasma sheet in response to IMF variations, *J. Geophys. Res.*, **119**, 3617–3640 (2014)

Collinson, G.A., A. Fedorov, Y. Futaana, K. Masunaga, R. Hartle, G. Stenberg, J. Grebowsky, M. Holmström, N. Andre, S. Barabash, T.-L. Zhang: The extension of ionospheric holes into the tail of Venus, *J. Geophys. Res.*, **119**, 6940–6953 (2014)

Collinson, G.A., D.G. Sibeck, A. Masters, N. Shane, T.-L. Zhang, A. Fedorov, S. Barabash, A.J. Coates, T.E. Moore, J.A. Slavin, V.M. Uritsky, S. Boardsen, M. Sarantos: A survey of hot flow anomalies at Venus, *J. Geophys. Res.*, **119**, 978–991 (2014)

Comisel, H., V. Constantinescu, Y. Narita: Origin of the filamentary structure in space plasmas, *Geosci. Lett.*, **1**, 12 (2014)

Comisel, H., Y. Narita, U. Motschmann: Wavevector anisotropy of plasma turbulence at ion kinetic scales: Solar wind observations and hybrid simulations, *Nonlin. Proc. Geophys.*, **21**, 1075–1083 (2014)

Delva, M., C. Bertucci, K. Schwingenschuh, M. Volwerk, N. Romanelli: Magnetic pileup boundary and field draping at Comet Halley, *Planet. Space Sci.*, **96**, 125–132 (2014)

Dubinin, E., M. Fraenz, T.-L. Zhang, J. Woch, Y. Wei: Magnetic fields in the Mars ionosphere of a non-crustal origin: Magnetization features, *Geophys. Res. Lett.*, **41**, 6329–6334 (2014)

Dubinin, E., M. Fraenz, T.-L. Zhang, J. Woch, Y. Wei: Magnetic fields in the Venus ionosphere: Dependence on the IMF direction – Venus Express observations, *J. Geophys. Res.*, **119**, 7587–7600 (2014)

Erkaev, N.V., C.J. Farrugia, A.V. Mezentsev, R.B. Torbert, H.K. Biernat: Slow mode structure in the nightside magnetosheath related to IMF draping, *J. Geophys. Res.*, **119**, 1121–1128 (2014)

Erkaev, N.V., H. Lammer, L.T. Elkins-Tanton, A. Stökl, P. Odert, E. Marcq, E.A. Dorfi, K.G. Kislyakova, Y.N. Kulikov, M. Leitzinger, M. Güdel: Escape of the martian protoatmosphere and initial water inventory, *Planet. Space Sci.*, **98**, 106–119 (2014)

Fischer, G., S.-Y. Ye, J.B. Groene, A.P. Ingersoll, K.M. Sayanagi, J.D. Menietti, W.S. Kurth, D.A. Gurnett: A possible influence of the Great White Spot on Saturn kilometric radiation periodicity, *Ann. Geophys.*, **32**, 1463–1476 (2014)

Forsyth, C., C.E.J. Watt, I.J. Rae, A.N. Fazakerley, N.M.E. Kalmoni, M.P. Freeman, P.D. Boakes, R. Nakamura, I. Dandouras, L.M. Kistler, C.M. Jackman, J.C. Coxon, C.M. Carr: Increases in plasma sheet temperature with solar wind driving during substorm growth phases, *Geophys. Res. Lett.*, **41**, 8713–8721 (2014)

Fossati, L., D. Bisikalo, H. Lammer, B. Shustov, M. Sachkov: Major prospects of exoplanet astronomy with the World Space Observatory – UltraViolet mission, *Astrophys. Space Sci.*, **354**, 9–19 (2014)

Gröller, H., H.I.M. Lichtenegger, H. Lammer, V.I. Shematovich: Hot oxygen and carbon escape from the martian atmosphere, *Planet. Space Sci.*, **98**, 93–105 (2014)

Jackman, C.M., C.S. Arridge, N. André, F. Bagenal, J. Birn, M.P. Freeman, X. Jia, A. Kidder, S.E. Milan, A. Radioti, J.A. Slavin, M.F. Vogt, M. Volwerk, A.P. Walsh: Large-scale structure and dynamics of the magnetotails of Mercury, Earth, Jupiter and Saturn, *Space Sci. Rev.*, **182**, 85–154 (2014)

Keiling, A., O. Marghitu, J. Vogt, O. Amm, C. Bunescu, V. Constantinescu, H. Frey, M. Hamrin, T. Karlsson, R. Nakamura, H. Nilsson, J. Semeter, E. Sorbalo: Magnetosphere-ionosphere coupling of global Pi2 pulsations, *J. Geophys. Res.*, **119**, 2717–2739 (2014)

Khutshishvili, E., V. Kulidzanishvili, T. Kvernadze, T.V. Zaqarashvili, V. Kakhiani, D. Khutsishvili, M. Sikharulidze: Quasi-periodic variations in Doppler velocities of H\alpha spicules, *Astrophys. Space Sci.*, **354**, 259–266 (2014)

Kislyakova, K.G., C.P. Johnstone, P. Odert, N.V. Erkaev, H. Lammer, T. Lüftinger, M. Holmström,

M.L. Khodachenko, M. Güdel: Stellar wind interaction and pick-up ion escape of the Kepler-11 "super-Earths", *Astron. Astrophys.*, **562**, A116 (2014)

Kislyakova, K.G., M. Holmström, H. Lammer, P. Odert, M.L. Khodachenko: Magnetic moment and plasma environment of HD 209458b as determined from Lyman-α observations, *Science*, **346**, 981-984 (2014)

Klinger, B., O. Baur, T. Mayer-Gürr: GRAIL gravity field recovery based on the short-arc integral equation technique: Simulation studies and first real data results, *Planet. Space Sci.*, **91**, 83-90 (2014)

Krauss, S., M. Pfleger, H. Lammer: Satellite-based analysis of thermosphere response to extreme solar flares, *Ann. Geophys.*, **32**, 1305-1309 (2014)

Kucharski, D., G. Kirchner, F. Koidl, C. Fan, R. Carman, Ch. Moore, A. Dmytrotsa, M. Ploner, G. Bianco, M. Medvedskij, A. Makeyev, G. Appleby, M. Suzuki, J.-M. Torre, Z. Zhongping, L. Grunwaldt, Q. Feng: Attitude and spin period of space debris Envisat measured by Satellite Laser Ranging, *IEEE Trans. Geosci. Rem. Sens.*, **52**, 7651-7657 (2014)

Kucharski, D., G. Kirchner, H.-C. Lim, F. Koidl: Spin parameters of High Earth Orbiting satellites Etalon-1 and Etalon-2 determined from kHz Satellite Laser Ranging data, *Adv. Space Res.*, **54**, 2309-2317 (2014)

Kucharski, D., H.-C. Lim, G. Kirchner, F. Koidl: Spin parameters of Low Earth Orbiting satellites Larets and Stella determined from Satellite Laser Ranging data, *Adv. Space Res.*, **53**, 90-96 (2014)

Kucharski, D., H.-C. Lim, G. Kirchner, T. Otsubo, G. Bianco, J.-Y. Hwang: Spin axis precession of LARES measured by satellite laser ranging, *IEEE Trans. Geosci. Rem. Sens.*, **11**, 646-650 (2014)

Lai, H., C.T. Russell, H. Wei, T.-L. Zhang: The evolution of co-orbiting material in the orbit of 2201 Oljato from 1980 to 2012 as deduced from Pioneer Venus Orbiter and Venus Express magnetic records, *Meteorit. Planet. Sci.*, **49**, 28-35 (2014)

Lammer, H., A. Stökl, N.V. Erkaev, E.A. Dorfi, P. Odert, M. Güdel, Yu.N. Kulikov, K.G. Kislyakova, M. Leitzinger: Origin and loss of nebula-captured hydrogen envelopes from 'sub'- to 'super-Earths' in the habitable zone of Sun-like stars, *MNRAS*, **438**, 3225-3238 (2014)

Lammer, H., S.-Ch. Schiefer, I. Juvan, P. Odert, N.V. Erkaev, Ch. Weber, K.G. Kislyakova, M. Güdel, G. Kirchengast, A. Hanslmeier: Origin and stability of Exomoon atmospheres: Implications for habitability, *Orig. Life Evol. Biosphere*, **44**, 239-260 (2014)

Leitzinger, M., P. Odert, R. Greimel, H. Korhonen, E.W. Guenther, A. Hanslmeier, H. Lammer, M.L. Khodachenko: A search for flares and mass ejections on young late-type stars in the open cluster Blanco-1, *MNRAS*, **443**, 898-910 (2014)

Li, S.-S., J. Liu, V. Angelopoulos, A. Runov, X.-Z. Zhou, S.A. Kiehas: Antidipolarization fronts observed by ARTEMIS, *J. Geophys. Res.*, **119**, 7181-7198 (2014)

Li, S.-S., V. Angelopoulos, A. Runov, S.A. Kiehas: Azimuthal extent and properties of midtail plasmoids from two-point ARTEMIS observations at the Earth-Moon Lagrange points, *J. Geophys. Res.*, **119**, 1781-1796 (2014)

Liu, Y.D., J.G. Luhmann, P. Kajdic, E.K.J. Kilpua, N. Lugaz, N.V. Nitta, Ch. Möstl, B. Lavraud, S.D. Bale, C.J. Farrugia, A.B. Galvin: Observations of an extreme storm in interplanetary space caused by successive coronal mass ejections, *Nat. Comm.*, **5**, 3481 (2014)

Lomineishvili, S.N., T.V. Zaqarashvili, I. Zhelyazkov, A.G. Tevzadze: Fast magnetohydrodynamic oscillation of longitudinally inhomogeneous prominence threads: an analogue with quantum harmonic oscillator, *Astron. Astrophys.*, **565**, A35 (2014)

Macher, W.: Transfer operator theory and inter-reciprocity of non-reciprocal multiport antennas, *Prog. Electromagn. Res. B*, **60**, 169-193 (2014)

Macher, W., N.I. Kömle, M.S. Bentley, G. Kargl: Temperature evolution of two parallel composite cylinders with contact resistances and application to thermal dual-probes, *Int. J. Heat Mass Transfer.*, **69**, 481-492 (2014)

Maier, A., S. Krauss, O. Baur: The role of Satellite Laser Ranging in terrestrial gravity field recovery, *Österr. Zeitschr. Verm. Geoinf.*, **102**, 3-10 (2014)

Masters, A., N. Achilleos, C.B. Agnor, S. Campagnola, S. Charnoz, B. Christophe, A.J. Coates, L.N. Fletcher, G.H. Jones, L. Lamy, F. Marzari, N. Nettelmann, J. Ruiz, R. Ambrosi, N. Andre, A. Bhardwaj, J.J. Fortney, C.J. Hansen, R. Helled, G.

Moragas-Klostermeyer, G. Orton, L. Ray, S. Reynaud, N. Sergis, R. Srama, M. Volwerk: Neptune and Triton: Essential pieces of the Solar System puzzle, *Planet. Space Sci.*, **104**, 108-121 (2014)

Melnik, V.N., A.I. Brazhenko, A.A. Konovalenko, H.O. Rucker, A.V. Frantsuzenko, V.V. Dorovskyy, M. Panchenko, A.A. Stanislavskyy: Unusual solar radio burst observed at decameter wavelengths, *Solar Phys.*, **289**, 263-278 (2014)

Melnik, V.N., N.V. Shevchuk, A.A. Konovalenko, H.O. Rucker, V.V. Dorovskyy, S. Poedts, A. Lecacheux: Solar decameter spikes, *Solar Phys.*, **289**, 1701-1714 (2014)

Morosan, D.E., P.T. Gallagher, P. Zucca, R. Fallows, E.P. Carley, G. Mann, M.M. Bisi, A. Kerdraon, A.A. Konovalenko, A.L. MacKinnon, H.O. Rucker, B. Thidé, J. Magdalenic, C. Vocks, H. Reid, J. Anderson, A. Asgekar, I.M. Avruch, M.J. Bentum, G. Bernardi, P. Best, A. Bonafede, J. Bregman, F. Breitling, J. Broderick, M. Brüggen, H.R. Butcher, B. Ciardi, J.E. Conway, F. de Gasperin, E. de Geus, A. Deller, S. Duscha, J. Eislöffel, D. Engels, H. Falcke, C. Ferrari, W. Frieswijk, M.A. Garrett, J. Grießmeier, A.W. Gunst, T.E. Hassall, J.W.T. Hessels, M. Hoeft, J. Hörandel, A. Horneffer, M. Iacobelli, E. Juette, A. Karastergiou, V.I. Kondratiev, M. Kramer, M. Kuniyoshi, G. Kuper, P. Maat, S. Markoff, J.P. McKean, D.D. Mulcahy, H. Munk, A. Nelles, M.J. Norden, E. Orru, H. Paas, M. Pandey-Pommier, V.N. Pandey, G. Pietka, R. Pizzo, A.G. Polatidis, W. Reich, H. Röttgering, A.M.M. Scaife, D. Schwarz, M. Serylak, O. Smirnov, B.W. Stappers, A. Stewart, M. Tagger, Y. Tang, C. Tasse, S. Thoudam, C. Toribio, R. Vermeulen, R.J. van Weeren, O. Wucknitz, S. Yatawatta, P. Zarka: LOFAR tied-array imaging of Type III solar radio bursts, *Astron. Astrophys.*, **568**, A67 (2014)

Möstl, Ch., K. Amla, J.R. Hall, P.C. Liewer, E.M. De Jong, R.C. Colaninno, A.M. Veronig, T. Rollett, M. Temmer, V. Peinhart, J.A. Davies, N. Lugaz, Y.D. Liu, C.J. Farrugia, J.G. Luhmann, B. Vrsnak, R.A. Harrison, A.B. Galvin: Connecting speeds, directions and arrival times of 22 Coronal Mass Ejections from the Sun to 1 AU, *Astrophys. J.*, **787**, 119 (2014)

Mousis, O., L.N. Fletcher, J.-P. Lebreton, P. Wurz, T. Cavalié, A. Coustenis, R. Courtin, D. Gautier, R. Helled, P.G.J. Irwin, A.D. Morse, N. Nettelmann, B. Marty, P. Rousselot, O. Venot, D.H. Atkinson, J.H. Waite, K.R. Reh, A.A. Simon, S. Atreya, N. André, M. Blanc, I.A. Daglis, G. Fischer, W.D. Geppert, T. Guillot, M.M. Hedman, R. Hueso, E. Lellouch, J.I. Lunine, C.D. Murray, J. O'Donoghue, M. Rengel, A. Sánchez-Lavega, F.-X. Schmider, A. Spiga, T. Spilker, J.-M. Petit, M.S. Tiscareno, M. Ali-Dib, K. Altwegg S.J. Bolton, A. Bouquet, C. Briois, T. Fouchet, S. Guerlet, T. Kostiuk, D. Lebleu, R. Moreno, G.S. Orton, J. Poncy: Scientific rationale for Saturn's in situ exploration, *Planet. Space Sci.*, **104**, 29-47 (2014)

Mousis, O., R. Hueso, J.-P. Beaulieu, S. Bouley.B. Carry, F. Colas, A. Klotz, C. Pellier, J.-M. Petit, P. Rousselot, M. Ali-Dib, W. Beisker, M. Birlan, C. Buil, A. Delsanti, E. Frappa, H.B. Hammel, A.C. Levasseur-Regourd, G.S. Orton, A. Sánchez-Lavega, A. Santerne, P. Tanga, J. Vaubaillon, B. Zanda, D. Baratoux, T. Böhm, V. Boudon, A. Bouquet, L. Buzzi, J.-L. Dauvergne, A. Decock, M. Delcroix, P. Drossart, N. Esseiva, G. Fischer, L.N. Fletcher, S. Foglia, J.M. Gómez-Forrellad, J. Guarro-Fló, D. Herald, E. Jehin, F. Kugel, J.-P. Lebreton, J. Lecacheux, A. Leroy, L. Maquet, G. Masi, A. Maury, F. Meyer, S. Pérez-Hoyos, A.S. Rajpurohit, C. Rinner, J.H. Rogers, F. Roques, R.W. Schmude Jr., B. Sicardy, B. Tregon, M. Vanhuysse, A. Wesley, T. Widemann: Instrumental methods for professional and amateur collaborations in planetary astronomy, *Exp. Astron.*, **38**, 91-191 (2014)

Moutou, C., J.M. Almenara, R.F. Diaz, R. Alonso, M. Deleuil, E. Guenther, T. Pasternacki, S. Aigrain, A. Baglin, P. Barge, A.S. Bonomo, P. Borde, F. Bouchy, J. Cabrera, S. Carpano, W.D. Cochran, Sz. Csizmadia, H.J. Deeg, R. Dvorak, M. Endl, A. Erikson, S. Ferraz-Mello, M. Fridlund, D. Gandolfi, T. Guillot, A. Hatzes, G. Hebrard, C. Lovis, H. Lammer, P.J. MacQueen, T. Mazeh, A. Ofir, M. Ollivier, M. Pätzold, H. Rauer, D. Rouan, A. Santerne, J. Schneider, B. Tingley, G. Wuchterl: CoRoT-22 b: A validated 4.9 R⊕ exoplanet in 10-d orbit, *MNRAS*, **444**, 2783-2792 (2014)

Nakamura, R., F. Plaschke, R. Teubenbacher, L. Giner, W. Baumjohann, W. Magnes, M. Steller, R.B. Torbert, H. Vaith, M. Chutter, K.-H. Fornaçon, K.-H. Glassmeier, C. Carr: Interinstrument calibration using magnetic field data from the Flux-Gate Magnetometer (FGM) and Electron Drift Instrument (EDI) onboard Cluster, *Geosci. Instrum. Method. Data Syst.*, **3**, 1-11 (2014)

Nakamura, R., T. Karlsson, M. Hamrin, H. Nilsson, O. Marghitu, O. Amm, C. Bunescu, V. Constantinescu, H.U. Frey, A. Keiling, J. Semeter, E. Sorbalo, J. Vogt, C. Forsyth, M.V. Kubyshkina: Low-altitude electron acceleration due to multiple flow bursts in the magnetotail, *Geophys. Res. Lett.*, **41**, 777-784 (2014)

Nakamura, T.K.M., W. Daughton: Turbulent plasma transport across the Earth's low-latitude boundary layer, *Geophys. Res. Lett.*, **41**, 8704-8712 (2014)

Narita, Y.: Four-dimensional energy spectrum for space-time structure of plasma turbulence, *Nonlin. Proc. Geophys.*, **21**, 41-47 (2014)

Narita, Y., H. Comisel, U. Motschmann: Spatial structure of ion-scale plasma turbulence, *Front. Physics*, **2**, 13 (2014)

Narita, Y., W. Baumjohann: Lessons on collisionless reconnection from quantum fluids, *Front. Physics*, **2**, 76 (2014)

Oliver, R., R. Soler, J. Terradas, T.V. Zaqarashvili, M.L. Khodachenko: Dynamics of coronal rain and descending plasma blobs in solar prominances. I. Fully ionized case, *Astrophys. J.*, **784**, 21 (2014)

Panchenko, M., W. Macher, H.O. Rucker, G. Fischer, T.H. Oswald, B. Cecconi, M. Maksimovic: In-flight calibration of STEREO-B/WAVES antenna system, *Radio Sci.*, **49**, 146-156 (2014)

Panov, E.V., W. Baumjohann, M.V. Kubyshkina, R. Nakamura, V.A. Sergeev, V. Angelopoulos, K.-H. Glassmeier, A.A. Petrukovich: On the increasing oscillation period of flows at the tailward retreating flux pileup region during dipolarization, *J. Geophys. Res.*, **119**, 6603-6611 (2014)

Panov, E.V., W. Baumjohann, R. Nakamura, M.V. Kubyshkina, K.-H. Glassmeier, V. Angelopoulos, A.A. Petrukovich, V.A. Sergeev: Period and damping factor of Pi2 pulsations during oscillatory flow braking in the magnetotail, *J. Geophys. Res.*, **119**, 4512-4520 (2014)

Perschke, Ch., Y. Narita, U. Motschmann, K.-H. Glassmeier: Multi-spacecraft observations of linear modes and sideband waves in ion-scale solar wind turbulence, *Astrophys. J. Lett.*, **793**, L25 (2014)

Plaschke, F., M.G.G.T. Taylor, R. Nakamura: Alternative interpretation of results from Kelvin-Helmholtz vortex identification criteria, *Geophys. Res. Lett.*, **41**, 244-250 (2014)

Plaschke, F., R. Nakamura, H.K. Leinweber, M. Chutter, H. Vaith, W. Baumjohann, M. Steller, W. Magnes: Flux-gate magnetometer spin axis offset calibration using the electron drift instrument, *Meas. Sci. Technol.*, **25**, 105008 (2014)

Prochazka, I., J. Kodet, J. Blazej, G. Kirchner, F. Koidl: Photon counting detector for space debris laser tracking and lunar laser ranging, *Adv. Space Res.*, **54**, 755-758 (2014)

Rauer, H., C. Catala, C. Aerts, T. Appourchaux, W. Benz, A. Brandeker, J. Christensen-Dalsgaard, M. Deleuil, L. Gizon, M.-J. Goupil, M. Güdel, E. Janot-Pacheco, M. Mas-Hesse, I. Pagano, G. Piotto, D. Pollacco, Ċ. Santos, A. Smith, J.-C. Suárez, R. Szabó, S. Udry, V. Adibekyan, Y. Alibert, J.-M. Almenara, P. Amaro-Seoane, M. Ammler-von Eiff, M. Asplund, E. Antonello, S. Barnes, F. Baudin, K. Belkacem, M. Bergemann, G. Bihain, A.C. Birch, X. Bonfils, I. Boisse, A.S. Bonomo, F. Borsa, I.M. Brandão, E. Brocato, S. Brun, M. Burleigh, R. Burston, J. Cabrera, S. Cassisi, W. Chaplin, S. Charpinet, C. Chiappini, R.P. Church, Sz. Csizmadia, M. Cunha, M. Damasso, M.B. Davies, H.J. Deeg, R.F. Díaz, S. Dreizler, C. Dreyer, P. Eggenberger, D. Ehrenreich, P. Eigmüller, A. Erikson, R. Farmer, S. Feltzing, F. de Oliveira Fialho, P. Figueira, T. Forveille, M. Fridlund, R.A. García, P. Giommi, G. Giuffrida, M. Godolt, J. Gomes da Silva, T. Granzer, J.L. Grenfell, A. Grotsch-Noels, E. Günther, C.A. Haswell, A.P. Hatzes, G. Hébrard, S. Hekker, R. Helled, K. Heng, J.M. Jenkins, A. Johansen, M.L. Khodachenko, K.G. Kislyakova, W. Kley, U. Kolb, N. Krivova, F. Kupka, H. Lammer, A.F. Lanza, Y. Lebreton, D. Magrin, P. Marcos-Arenal, P.M. Marrese, J.P. Marques, J. Martins, S. Mathis, S. Mathur, S. Messina, A. Miglio, J. Montalban, M. Montalto, M.J.P.F.G. Monteiro, H. Moradi, E. Moravveji, C. Mordasini, T. Morel, A. Mortier, V. Nascimbeni, R.P. Nelson, M.B. Nielsen, L. Noack, A.J. Norton, A. Ofir, M. Oshagh, R.-M. Ouazzani, P. Pápics, V.C. Parro, P. Petit, B. Plez, E. Poretti, A. Quirrenbach, R. Ragazzoni, G. Raimondo, M. Rainer, D.R. Reese, R. Redmer, S. Reffert, B. Rojas-Ayala, I.W. Roxburgh, S. Salmon, A. Santerne, J. Schneider, J. Schou, S. Schuh, H. Schunker, A. Silva-Valio, R. Silvotti, I. Skillen, I. Snellen, F. Sohl, S.G. Sousa, A. Sozzetti,

D. Stello, K.G. Strassmeier, M. Švanda, Gy.M. Szabó, A. Tkachenko, D. Valencia, V. Van Grootel, S.D. Vauclair, P. Ventura, F.W. Wagner, N.A. Walton, J. Weingrill, S.C. Werner, P.J. Wheatley, K. Zwintz: The PLATO 2.0 mission, *Exp. Astron.*, **38**, 249–330 (2014)

Rollett, T., Ch. Möstl, M. Temmer, R.A. Frahm, J.A. Davies, A.M. Veronig, B. Vrsnak, U.V. Amerstorfer, C.J. Farrugia, T. Zic, T.–L. Zhang: Combined multipoint remote and in situ observations of the asymmetric evolution of a fast solar coronal mass ejection, *Astrophys. J. Lett.*, **790**, L6 (2014)

Romanelli, N., D. Gomez, C. Bertucci, M. Delva: Steady–state magnetohydrodynamic flow around an unmagnetized conducting sphere, *Astrophys. J.*, **789**, 43 (2014)

Rong, Z.J., S. Barabash, Y. Futaana, G. Stenberg, T.–L. Zhang, W.X. Wan, Y. Wei, X.–D. Wang, L.H. Chai, J. Zhong: Morphology of magnetic field in near–Venus magnetotail: Venus Express observations, *J. Geophys. Res.*, **119**, 8838–8847 (2014)

Rong, Z.J., W.X. Wan, C. Shen, A.A. Petrukovich, W. Baumjohann, M.W. Dunlop, Y.C. Zhang: Radial distribution of magnetic field in earth magnetotail current sheet, *Planet. Space Sci.*, **103**, 273–285 (2014)

Rozhnoi, A., M. Solovieva, V. Fedun, M. Hayakawa, K. Schwingenschuh, B. Levin: Correlation of very low and low frequency signal variations at mid–latitudes with magnetic activity and outer–zone particles, *Ann. Geophys.*, **32**, 1455–1462 (2014)

Rucker, H.O., M. Panchenko, C. Weber: Planetary radio astronomy: Earth, giant planets, and beyond, *Adv. Radio Sci.*, **12**, 221–220 (2014)

Sampl, M., W. Macher, C. Gruber, T. Oswald, M. Kapper, H.O. Rucker, M. Mogilevsky: HF performance of electric field sensors aboard the RESONANCE satellite, *Geosci. Instrum. Method. Data Syst. Disc.*, **4**, 683–703 (2014)

Schmid, D., M. Volwerk, F. Plaschke, Z. Vörös, T.–L. Zhang, W. Baumjohann, Y. Narita: Mirror mode structures near Venus and comet P/Halley, *Ann. Geophys.*, **32**, 651–657 (2014)

Seo, Y.K., D.Y. Rew, G. Kirchner, E. Park, M. Choi, S.Y. Yu, J. Heo, C. Youn: A new approach to the telescope operation method for satellite tracking using a time synchronization technique, *Adv. Space Res.*, **54**, 1467–1478 (2014)

Sergeev, V.A., A.V. Nikolaev, M.V. Kubyshkina, N.A. Tsyganenko, H.J. Singer, J.V. Rodriguez, V. Angelopoulos, R. Nakamura, S.E. Milan, J.C. Coxon, B.J. Anderson, H. Korth: Event study combining magnetospheric and ionospheric perspectives of the substorm current wedge modeling, *J. Geophys. Res.*, **119**, 9714–9728 (2014)

Sergeev, V.A., I.A. Chernyaev, V. Angelopoulos, A.V. Runov, R. Nakamura: Stopping flow bursts and their role in the generation of the substorm current wedge, *Geophys. Res. Lett.*, **41**, 1106–1112 (2014)

Shaikhislamov, I.F., M.L. Khodachenko, Yu.L. Sasunov, H. Lammer, K.G. Kislyakova, N.V. Erkaev: Atmosphere expansion and mass loading of close–orbit giant exoplanets heated by stellar XUV. I. Modeling of hydrodynamic escape of upper atmospheric material, *Astrophys. J.*, **795**, 132 (2014)

Shan, L., Q. Lu, M. Wu, X. Gao, C. Huang, T. Zhang, S. Wang: Transmission of large–amplitude ULF waves through a quasi–parallel shock at Venus, *J. Geophys. Res.*, **119**, 237–245 (2014)

Sharma, R.P., R. Goyal, E.E. Scime, N.K. Dwivedi: Localization of linear kinetic Alfvén wave in an inhomogeneous plasma and generation of turbulence, *Phys. Plasmas*, **21**, 042113 (2014)

Shematovich, V.I., D.E. Ionov, H. Lammer: Heating efficiency in hydrogen–dominated upper atmospheres, *Astron. Astrophys.*, **571**, A94 (2014)

Shi, J., Z. Zhang, K. Torkar, M. Dunlop, A. Fazakerley, Z. Cheng, Z. Liu: Temporal and spatial scales of a high–flux electron disturbance in the cusp region: Cluster observations, *J. Geophys. Res.*, **119**, 4536–4543 (2014)

Teh, W.–L., R. Nakamura, H. Karimabadi, W. Baumjohann, T.–L. Zhang: Correlation of core field polarity of magnetotail flux ropes with the IMF By: Reconnection guide field dependency, *J. Geophys. Res.*, **119**, 2933–2944 (2014)

Thomsen, M.F., D.B. Reisenfeld, R.J. Wilson, M. Andriopoulou, F.J. Crary, G.B. Hospodarsky, C.M. Jackman, X. Jia, K.K. Khurana, C. Paranicas, E. Roussos, N. Sergis, R.L. Tokar: Ion composition in interchange injection events in Saturn's magnetosphere, *J. Geophys. Res.*, **119**, 9761–9772 (2014)

Treumann, R.A., W. Baumjohann: Beyond Gibbs–Boltzmann–Shannon: General entropies – the Gibbs–Lorentzian example, *Front. Physics*, **2**, 49 (2014)

Treumann, R.A., W. Baumjohann: Brief Communication: Weibel, firehose and mirror mode relations, *Nonlin. Proc. Geophys.*, **21**, 143–148 (2014)

Treumann, R.A., W. Baumjohann: Fractional Laplace transforms – a perspective, *Front. Physics*, **2**, 29 (2014)

Treumann, R.A., W. Baumjohann: Plasma wave mediated attractive potentials: a prerequisite for electron compound formation, *Ann. Geophys.*, **32**, 975–989 (2014)

Treumann, R.A., W. Baumjohann: Superdiffusion revisited in view of collisionless reconnection, *Ann. Geophys.*, **32**, 643–650 (2014)

Treumann, R.A., W. Baumjohann, A. Balogh: The strongest magnetic fields in the universe: How strong can they become?, *Front. Physics*, **2**, 59 (2014)

Vasko, I.Y., A.V. Artemyev, A.A. Petrukovich, R. Nakamura, L.M. Zelenyi: The structure of strongly tilted current sheets in the Earth magnetotail, *Ann. Geophys.*, **32**, 133–146 (2014)

Vasko, I.Y., L.M. Zelenyi, A.V. Artemyev, A.A. Petrukovich, H.V. Malova, T.–L. Zhang, A.O. Fedorov, V.Y. Popov, S. Barabash, R. Nakamura: The structure of the Venusian current sheet, *Planet. Space Sci.*, **96**, 81–89 (2014)

Volwerk, M., K.–H. Glassmeier, M. Delva, D. Schmid, C. Koenders, I. Richter, K. Szegö: A comparison between VEGA 1, 2 and Giotto flybys of comet 1P/Halley: Implications for Rosetta, *Ann. Geophys.*, **32**, 1441–1453 (2014)

Vörös, Z., G. Facskó, M.L. Khodachenko, I. Honkonen, P. Janhunen, M. Palmroth: Windsock memory COnditioned RAM (CO–RAM) pressure effect: Forced reconnection in the Earth's magnetotail, *J. Geophys. Res.*, **119**, 6273–6293 (2014)

Vörös, Z., Yu.L. Sasunov, V.S. Semenov, T.V. Zaqarashvili, R. Bruno, M.L. Khodachenko: Reconnection outflow generated turbulence in the solar wind, *Astrophys. J. Lett.*, **797**, L10 (2014)

Vrsnak, B., M. Temmer, T. Zic, A. Taktakishvili, M. Dumbovic, Ch. Möstl, A.M. Veronig, M.L. Mays, D. Odstrcil: Heliospheric propagation of Coronal Mass Ejections: Comparison of numerical WSA–Enlil+Cone Model and analytic drag–based model, *Astrophys. J. Suppl. Ser.*, **213**, 21 (2014)

Wang, C.P., X. Xing, T.K.M. Nakamura, L.R. Lyons, V. Angelopoulos: Source and structure of bursty hot electron enhancements in the tail magnetosheath: Simultaneous two–probe observation by ARTEMIS, *J. Geophys. Res.*, **119**, 9900–9918 (2014)

Wang, G.Q., M. Volwerk, R. Nakamura, P. Boakes, T.L. Zhang, A. Yoshikawa, D.G. Baishev: Flapping current sheet with superposed waves seen in space and on the ground, *J. Geophys. Res.*, **119**, 10078–10091 (2014)

Wang, R., Q. Lu, A. Du, R. Nakamura, S. Lu, C. Huang, C. Liu, M. Wu: In situ observation of magnetic reconnection in the front of bursty bulk flow, *J. Geophys. Res.*, **119**, 9952–9961 (2014)

Wang, R., Q. Lu, Y.V. Khotyaintsev, M. Volwerk, A. Du, R. Nakamura, W.D. Gonzalez, X. Sun, W. Baumjohann, X. Li, T.–L. Zhang, A.N. Fazakerley, C. Huang, M. Wu: Observation of double layer in the separatrix region during magnetic reconnection, *Geophys. Res. Lett.*, **41**, 4851–4858 (2014)

Wang, R., R. Nakamura, T. Zhang, A. Du, W. Baumjohann, Q. Lu, A.N. Fazakerley: Evidence of transient reconnection in the outflow jet of primary reconnection site, *Ann. Geophys.*, **32**, 239–248 (2014)

Wang, Z., J. Shi, Y. Guan, C. Liu, G. Zhu, K. Torkar, M. Friedrich: A model for the sounding rocket measurement on an ionospheric E–F valley at the Hainan low latitude station, *Plasma Sci. Technol.*, **16**, 316–319 (2014)

Wang, Z., J.K. Shi, K. Torkar, G.J. Wang, X. Wang: Correlation between ionospheric strong range spread F and scintillations observed in Vanimo station, *J. Geophys. Res.*, **119**, 8578–8585 (2014)

Webb, D.F., M.M. Bisi, C.A. de Koning, C.J. Farrugia, B.V. Jackson, L.K. Jian, N. Lugaz, K. Marubashi, Ch. Möstl, E.P. Romashets, B.E. Wood, H.–S. Yu: An ensemble study of a January 2010 Coronal Mass Ejection (CME): Connecting a non–obvious Solar source with its ICME/magnetic cloud, *Solar Phys.*, **289**, 4173–4208 (2014)

Wilczek, M., H. Xu, Y. Narita: A note on Taylor's hypothesis under large–scale flow variation, *Nonlin. Proc. Geophys.*, **21**, 645–649 (2014)

Wilczek, M., R.J.A.M. Stevens, Y. Narita, Ch. Meneveau: A wavenumber–frequency spectral model for atmospheric boundary layers, *J. Phys. Conf. Ser.*, **524**, 012104 (2014)

Zaqarashvili, T.V., Z. Vörös, I. Zhelyazkov: Kelvin-Helmholtz instability of twisted magnetic flux tubes in the solar wind, *Astron. Astrophys.*, **561**, A62 (2014)

Zaqarashvili, T.V., Z. Vörös, Y. Narita, R. Bruno: Twisted magnetic flux tubes in the solar wind, *Astrophys. J. Lett.*, **783**, L19 (2014)

Books

Kömle, N.I., G. Fischer, W. Macher (Eds.): PRE 7.5, Planetary Retirement Edition, Living Edition, Pöllauberg, 154 pages, 2014

Proceedings & Book Chapters

Baumjohann, W.: Altes und Neues aus der Weltraumphysik. In: *Nachhaltige Entwicklungen an der TU Graz und ihre Initiatoren. Sechzehn Wissenschaftsportrits*, Ed. Forum Technik und Gesellschaft, Verlag der Technischen Universität Graz, Graz, CD: 11-12 (2014)

Baumjohann, W.: Das Grazer Institut für Weltraumforschung: ein Profil. In: *Steirisches Jahrbuch für Politik 2013*, Eds. Karl, B., W. Mantl, K. Poier, A. Prettenthaler-Ziegerhofer, M. Prisching, B. Schilcher, Böhlau, Wien, 159-162 (2014)

Baumjohann, W.: Grußadresse. In: *PRE 7.5, Planetary Retirement Edition*, Eds. Kömle, N.I., G. Fischer, W. Macher, Living Edition, Pöllauberg, 5-6 (2014)

Becker, U., U. Bergner, B.P. Besser: Grazer Mathematikerkreis. In: *Idee und From. Mathematik und die Schönheit der Wissenschaft*, Eds. Peer, P., H. Hensle-Wlasak, U. Becker, P. Pakesch, Universalmuseum Joanneum, Graz, 16-17 (2014)

Besser, B.P.: Das Engagement österreichischer Unternehmen in der Weltraumtechnologie - Kurze Geschichte bis zum Jahr 2005. In: *Zeitenblicke - 100 Jahre Wirtschaft in der Steiermark. Wirtschaftspolitische Blätter, Sonderausgabe 2014*, Ed. Wirtschaftskommer Österreich, Manz, Wien, 65-74 (2014)

Besser, B.P.: Österreichs Weg in den Weltraum bis 1968. In: *Nachhaltige Entwicklungen an der TU Graz und ihre Initiatoren. Sechzehn Wissenschaftsportrits*, Ed. Forum Technik und Gesellschaft, Verlag der Technischen Universität Graz, Graz, CD: 6-7 (2014)

Besser, B.P., H. Hensle-Wlasak, U. Becker: Den Raum vermessen. In: *Idee und From. Mathematik und die Schönheit der Wissenschaft*, Eds. Peer, P., H. Hensle-Wlasak, U. Becker, P. Pakesch, Universalmuseum Joanneum, Graz, 10-11 (2014)

Besser, B.P., U. Becker: Den Himmel erforschen. In: *Idee und From. Mathematik und die Schönheit der Wissenschaft*, Eds. Peer, P., H. Hensle-Wlasak, U. Becker, P. Pakesch, Universalmuseum Joanneum, Graz, 14-15 (2014)

Biernat, H.K.: Grußadresse. In: *PRE 7.5, Planetary Retirement Edition*, Eds. Kömle, N.I., G. Fischer, W. Macher, Living Edition, Pöllauberg, 7-8 (2014)

Boudjada, M.Y.: Ground-based observations at Lustbühel radio station. In: *PRE 7.5, Planetary Retirement Edition*, Eds. Kömle, N.I., G. Fischer, W. Macher, Living Edition, Pöllauberg, 43-54 (2014)

Dvorak, R., Ch. Lhotka: Sitnikov problem. In: *Scholarpedia*, www.scholarpedia.org, online, 9 (12) 11096, doi:10.4249/scholarpedia.11096 (2014)

Fischer, G., W. Macher, M. Panchenko: Space-based radio observations of Saturn at IWF. In: *PRE 7.5, Planetary Retirement Edition*, Eds. Kömle, N.I., G. Fischer, W. Macher, Living Edition, Pöllauberg, 55-70 (2014)

Güdel, M., R. Dvorak R., N.V. Erkaev, J. Kasting, M.L. Khodachenko, H. Lammer, E. Pilat-Lohinger, H. Rauer, T. Ribas, B. Wood: Astrophysical conditions for planetary habitability. In: *Protostars and Planets VI*, Eds. Beuther, H., R.S. Klessen, C.P. Dullemond, T. Henning, University of Arizona Press, Tucson, 883-906 (2014)

Hensle-Wlasak, H., B.P. Besser: Die andere Seite der Wissenschaft. In: *Idee und From. Mathematik und die Schönheit der Wissenschaft*, Eds. Peer, P., H. Hensle-Wlasak, U. Becker, P. Pakesch, Universalmuseum Joanneum, Graz, 18-19 (2014)

Hensle-Wlasak, H., B.P. Besser: Zahlenwelten. In: *Idee und From. Mathematik und die Schönheit der Wissenschaft*, Eds. Peer, P., H. Hensle-Wlasak, U. Becker, P. Pakesch, Universalmuseum Joanneum, Graz, 8-9 (2014)

Hensle-Wlasak, H., B.P. Besser, U. Becker: Die Zeit teilen. In: *Idee und From. Mathematik und die Schönheit der Wissenschaft*, Eds. Peer, P., H. Hensle-Wlasak, U. Becker, P. Pakesch, Universalmuseum Joanneum, Graz, 12-13 (2014)

Khodachenko, M.L., Europlanet Team: European FP6, FP7 projects Europlanet and Europlanet-RI – a crucial step towards integration of the European planetary science. In: *PRE 7.5, Planetary Retirement Edition*, Eds. Kömle, N.I., G. Fischer, W. Macher, Living Edition, Pöllauberg, 89-95 (2014)

Khodachenko, M.L., Yu.L. Sasunov, O.V. Arkhypov, I.I. Alexeev, E.S. Belenkaya, H. Lammer, K.G. Kislyakova, P. Odert, M. Leitzinger, M. Güdel: Stellar CME activity and its possible influence on exoplanets' environments: Importance of magnetospheric protection. In: *Nature of Prominences and their role in Space Weather. Proceedings of the International Astronomical Union, Volume 8, Symposium S300*, Eds. Schmieder, B., J.-M. Malherbe, S.T. Wu, Cambridge University Press, Cambridge, UK, 335-346, doi:10.1017/S1743921313011174 (2014)

Kömle, N.I.: Grußadresse. Helmut's gesammelte Werke. In: *PRE 7.5, Planetary Retirement Edition*, Eds. Kömle, N.I., G. Fischer, W. Macher, Living Edition, Pöllauberg, 105-109 (2014)

Kömle, N.I., G. Fischer, W. Macher: Publication list of Prof. Helmut O. Rucker. In: *PRE 7.5, Planetary Retirement Edition*, Eds. Kömle, N.I., G. Fischer, W. Macher, Living Edition, Pöllauberg, 129-154 (2014)

Korovinskiy, D., A. Divin, V. Ivanova, N.V. Erkaev, V.S. Semenov, I. Ivanov, H.K. Biernat, G. Lapenta, S. Markidis: MHD modeling of the kink "double-gradient" branch of the ballooning instability in the magnetotail. In: *Proceedings 8th International Conference of "Numerical Modeling of Space Plasma Flows: ASTRONUM-2013", ASP Conference Series, 488*, Ed. Pogorelov N.V, E. Audit, G. P. Zank, Astronomical Society of the Pacific (ASP), San Francisco, 149-154 (2014)

Lammer, H., M. Panchenko, C. Weber: Attempts to observe radio emissions from planets beyond our solar system. In: *PRE 7.5, Planetary Retirement Edition*, Eds. Kömle, N.I., G. Fischer, W. Macher, Living Edition, Pöllauberg, 79-88 (2014)

Macher, W., M. Sampl, M. Kapper, G. Fischer, M. Panchenko: Panta rheometry. In: *PRE 7.5, Planetary Retirement Edition*, Eds. Kömle, N.I., G. Fischer, W. Macher, Living Edition, Pöllauberg, 21-41 (2014)

Panchenko, M., G. Fischer, W. Macher: Space-based observations of Jupiter's radio emission at IWF. In: *PRE 7.5, Planetary Retirement Edition*, Eds. Kömle, N.I., G. Fischer, W. Macher, Living Edition, Pöllauberg, 71-78 (2014)

Sneeuw, N., J. Li, O. Baur, J. Cai, M.J. Tourian, O. Elmi, W. Jiang, Y. Chu, T. Jin, H. Wirnsberger, A. Krauss, A. Maier: Current and future geodetic satellite missions for global change monitoring. In: *Proceedings "Dragon 3 Mid-Term Symposium", ESA SP-724*, ESA Publ. Div., Noordwijk, 6 p. (2014)

Sünkel, H.: Satellitengeodäsie und Weltraumforschung. In: *Lebenszeugnisse österreichischer Vizekanzler: Das politische System*, Ed. Mantl, W., Böhlau, Wien, n - n+6 (2014)

Torkar, K., R. Nakamura: Interdependencies between the actively controlled CLUSTER spacecraft potential, ambient plasma, and electric field Measurements. In: *Proceedings of the 13th Spacecraft Charging Technology Conference*, Jet Propulsion Laboratory, Pasadena, 26 p. (2014)

For oral presentations and posters please refer to www.iwf.oeaw.ac.at/en/publications.

Personnel

Alexandrova, Alexandra, MSc
Almer Hannes
Al-Ubaidi, Tarek, Dipl.-Ing.
Andriopoulou Maria, Dr.
Arkhypov, Oleksiy, Dr.
Aydogar, Özer, Dipl.-Ing.
Baumjohann, Wolfgang, Prof.
Baur, Oliver, Dr.
Bentley, Mark, Dr.
Berghofer, Gerhard, Ing.
Besser, Bruno P., Dr.
Boudjada, Mohammed Y., Dr.
Bourdin, Philippe, Dr.
Delva, Magda, Dr.
Dwivedi, Navin, Dr.
Eichelberger, Hans U., Dipl.-Ing.
Fischer, David, Dipl.-Ing.
Fischer, Georg, Dr.
Flock, Barbara, Mag.
Fremuth, Gerhard, Dipl.-Ing.
Giner, Franz, Dipl.-Ing.
Graf, Christian, Ing.
Grill, Claudia
Hagen, Christian, Dipl.-Ing.
Hasiba, Johann, Dipl.-Ing.
Hofmann, Karl, Dipl.-Ing.
Höck, Eduard, Dipl.-Ing.
Hradecky, Doris
Jernej, Irmgard, Ing.
Jeszenszky, Harald, Dipl.-Ing.
Kapper, Michael, Dr.
Kargl, Günter, Dr.
Khodachenko, Maxim L., Dr.
Kirchner, Georg, Dr.
Kislyakova, Kristina, Dr.
Koidl, Franz, Ing.
Kömle, Norbert I., Doz.
Krauss, Sandro, Dr.
Kürbisch, Christoph, Ing.
Laky, Gunter, Dipl.-Ing.
Lammer, Helmut, Dr.
Leichtfried, Mario, Ing.
Leitner, Stefan, Dipl.-Ing.
Lichtenegger, Herbert I.M., Dr.
Lhotka Christoph, Dr.
Macher, Wolfgang, Dr.
Magnes, Werner, Dr.
Močnik, Karl, Dr.
Möstl Christian, Dr.
Nakamura, Rumi, Doz.
Nakamura, Takuma, Dr.
Narita, Yasuhito, Doz.
Neukirchner, Sonja, Ing.
Nischelwitzer-Fennes, Ute, Ing.
Ottacher, Harald, Dipl.-Ing.
Pagaran, Joseph A., Dr.
Panchenko, Mykhaylo, Dr.
Panov, Evgeny, Dr.
Pitterle, Martin
Plaschke, Ferdinand, Dr.
Poganski Joshua
Pollinger, Andreas, Dr.
Prattes, Gustav, Dipl.-Ing.
Rollett, Tanja, Dr.
Sasunov, Jury, Dr.
Scherf, Manuel, Mag.
Scherr, Alexandra, Mag.
Schmid, Daniel, Dipl.-Ing.
Schmied Roland
Shergelashvili Bidzina, Dr.
Stachel, Manfred, Dipl.-Ing.
Stangl, Günter, Dr. (BEV)
Steinberger, Michael, Dipl.-Ing.
Steller, Manfred B., Dr.
Stieninger, Reinhard, Ing.
Topf, Florian, BSc
Valavanoglou, Aris, Dipl.-Ing.
Voller, Wolfgang G., Mag.
Volwerk, Martin, Dr.
Vörös, Zoltán, Dr.
Wallner, Robert, Ing.
Wang, Peiyuan, Dr.
Weber, Christof, Mag.
Wirnsberger, Harald, Dipl.-Ing.
Zaqarashvili, Teimuraz, Dr.
Zehetleitner, Sigrid, Mag.
Zhang, Tie-Long, Prof.

As of 31 December 2014

BEV: Federal Office for Metrology and Surveying

Impressum

Published by
IWF Director

Compiled and designed by
IWF Public Relations

Printed by
Druckwerk, 8020 Graz

Institut für Weltraumforschung (IWF)
Österreichische Akademie der Wissenschaften (ÖAW)
Schmiedlstraße 6
8042 Graz, Austria
T +43 316 4120-400
pr.iwf@oeaw.ac.at
www.iwf.oeaw.ac.at
@IWF_Graz